Journal of Energy Resources Technology. Received September 16, 2022;
Accepted manuscript posted December 31, 2022. doi:10.1115/1.4056612




# Carbon dioxide Sequestration in Low Porosity and Permeability Deep Saline Aquifer: Numerical Simulation Method

Grant Charles Mwakipunda[1, *], Mbega Ramadhani Ngata[1], Melckzedeck Michael Mgimba[1,2], Long Yu[1,**]

1. Key Laboratory of Theory and Technology of Petroleum Exploration and Development in Hubei Province, China University of Geosciences, Wuhan 430074, China

2. Mbeya University of Science and Technology (MUST), P.O Box 131, Mbeya, Tanzania

[*]Corresponding author Email: grantmwakipunda@hotmail.com

[**]Corresponding author Email: yulong36@cug.edu.cn





## Abstract

The saline aquifer is the most reliable place where anthropogenic carbon dioxide gas storage has shown a promising future. This paper evaluates and predicts the capacities of different carbon dioxide storage trapping mechanisms in storing carbon dioxide gas in low porosity and permeability deep saline aquifers by using commercial reservoir simulator software i.e., Computer modeling group (CMG). Four carbon dioxide storage trapping modeled and simulated were: structural or stratigraphic trapping mechanisms, residual trapping mechanisms, solubility trapping mechanisms, and mineral trapping mechanisms. Carbon dioxide gas was injected into a deep saline aquifer for 15 years, followed by 833 years of post-injection. To reflect the real field reality and have a reasonable approximation of the amount of carbon dioxide which can be stored in an aquifer, this paper included water vaporization effects which occur during carbon dioxide injection and water injection operations so as to optimize residual and solubility trapping mechanisms as the most important trapping mechanisms. Furthermore, the effects of different important parameters such as salinity, vertical to horizontal permeability ratio, injection rate, bottom hole pressure, and temperature on each carbon dioxide trapping mechanism were analyzed. Results revealed that each carbon dioxide trapping mechanism has a different capacity for storing carbon dioxide and could be either affected linearly or non-linearly with various parameters. Higher aquifer temperatures are not recommended for carbon dioxide storage because most of the carbon dioxide gas is stored as free gas, which increases the risk of leakage in case of mechanical failure or imbalance. Excess salinity is the only factor that reduces aquifer storage capacity. Furthermore, it was found that an aquifer with a lower vertical to horizontal permeability ratio is recommended for carbon dioxide storage because it increases carbon dioxide stored in an immobile phase, which avoids risk leakages i.e., There was an increase of 43.2% and a decrease of 16.84% for minimum and maximum vertical to horizontal permeability ($k_v/k_h$) ratios, respectively, compared to the base for residual trapping mechanisms. Also, there was a decrease of carbon dioxide dissolved by 19% at maximum $k_v/k_h$ ratios and an increase of 58% at minimum $k_v/k_h$ ratios, compared to the base case. Further, there was an increase of carbon dioxide trapped by 96.4% and dissolved by 97% when water was injected at a higher rate compared to the base case (no water injection). Thus, a

Journal of Energy Resources Technology. Received September 16, 2022;
Accepted manuscript posted December 31, 2022. doi:10.1115/1.4056612


high injection rate is suggested to enhance residual and solubility trapping mechanisms. It is recommended that the carbon dioxide injection rate and bottom hole pressure be kept at optimal levels to avoid mechanical failure due to aquifer pressures building up, which can increase the risk of leakages and must be monitored and controlled at the surface using pressure gauges or sensor technology.

Key words: Deep saline aquifer; Trapping mechanisms; Low porosity and permeability; Carbon dioxide sequestration.

## 1. Introduction

In recent years, there has been a massive increase in the emissions of carbon dioxide and greenhouse gases (GHGs) in the atmosphere due to major developments in heavy industries like cement industries, which release (2.4 $GtCO_2$), chemical industries (1.4 $GtCO_2$), iron and steel industries (2.6 $GtCO_2$), power and transportation industries per year etc. The increase of these gases in the atmosphere has caused global warming and unpredicted climatic changes. Between 2017 and 2018, there was a 2.7% (37.1 Gt) increase in carbon in the atmosphere as a result of fossil fuel use [1-5]. Currently, $CO_2$ levels in the atmosphere are more than 412 parts per million (ppm) and still rising. Carbon Capture, Utilization, and Storage (CCUS) is the key technology that, if implemented on a large scale globally, has the potential to reduce carbon dioxide and greenhouse gases emissions in the atmosphere to achieve the primary mitigation strategy for Paris climate summit agreement to achieve net zero greenhouse gas (GHG) emissions by 2050 and a maximum global temperature increase of 1.5 degrees Celsius[6-9]. CCUS entails capture carbon from different sources and either store it in depleted hydrocarbons reservoirs/saline aquifers or supplying it for other uses in other production industries such as raw materials and converting it into value-added products such as polymers, building materials, chemicals and synthetic fuels, using it directly in soft drinks, and in carbon dioxide enhanced oil recovery ($CO_2$-EOR) etc. as summarized in Fig. 1. Instead, the majority of the carbon dioxide gases are released into the atmosphere, limiting the Paris climate summit agreement to reach net zero GHG emissions [6, 10-13]. There are various technologies which are employed in capturing carbon dioxide from different sources as explained by Hong [12] and summarized in Fig. 2[14, 15].Geological options for carbon dioxide storage have different capacity storage and associated risks as shown in Table 1[16, 17].Deep saline aquifer is the most preferred and used option for carbon dioxide storage as reported by the European Zero Emission Platform (ZEP) as summarized in Fig. 3 [17, 18].It has capacity of storing carbon dioxide gases up to 10,000 Gt globally. The aquifer characteristics that are suitable for carbon dioxide are summarized in Table 2.

Journal of Energy Resources Technology. Received September 16, 2022;
Accepted manuscript posted December 31, 2022. doi:10.1115/1.4056612


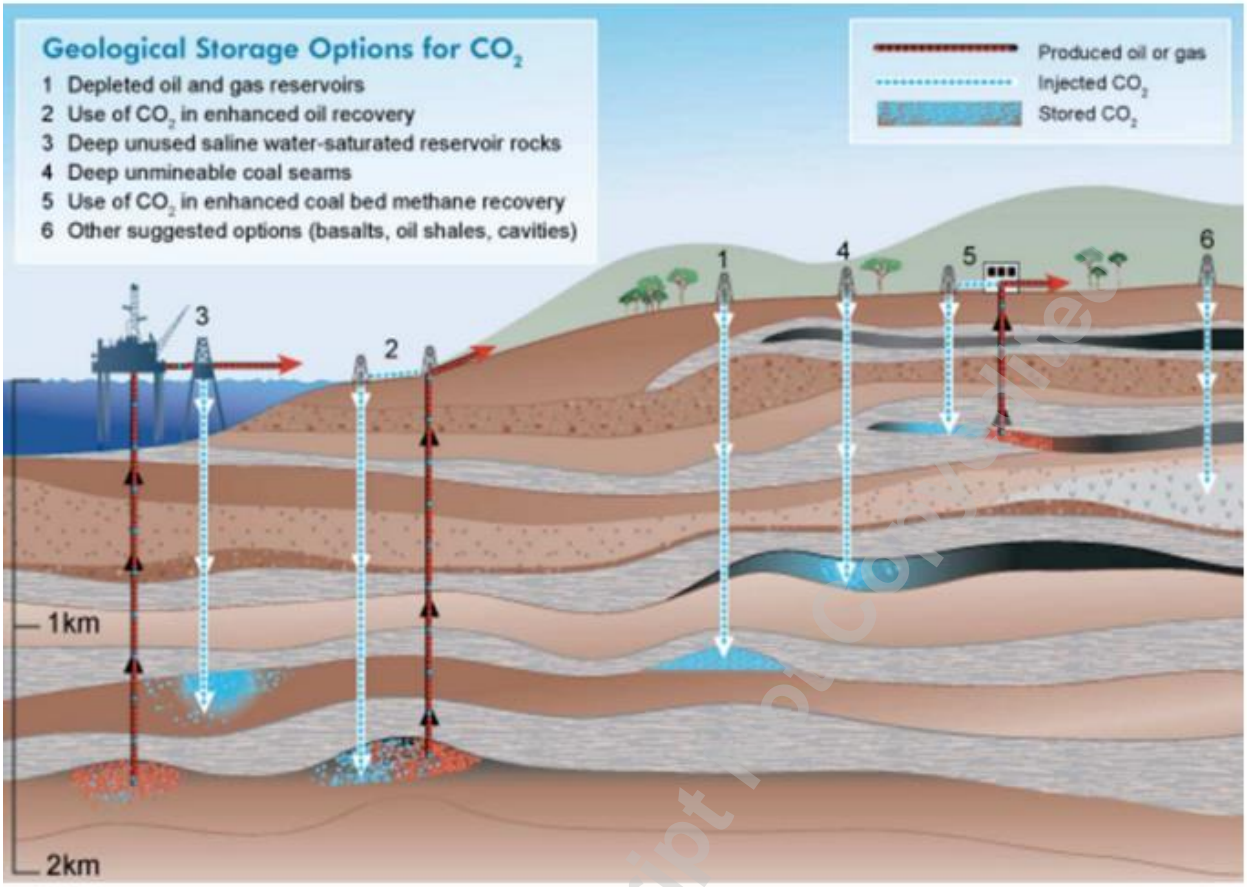


**Fig. 1** Geological storage options for $CO_2$ [19].

Table 1 Different carbon dioxide options, capacities and their associated risks in USA [16, 17].

| Storage options | Capacity (Gt-$CO_2$) | Storage integrity | Environmental risk |
|---|---|---|---|
| Depleted oil and gas fields | 25-30 | High | Low |
| Active oil wells (EOR) | Low | High | Low |
| Enhanced coal-bed methane | 5-10 | Medium | Medium |
| Deep aquifers | 1-150 | Medium | Medium |
| Ocean (global) | 1000-10,000 | Medium | High |
| Carbonate storage (No transport) | Very high | Highest | High |

Journal of Energy Resources Technology. Received September 16, 2022;
Accepted manuscript posted December 31, 2022. doi:10.1115/1.4056612


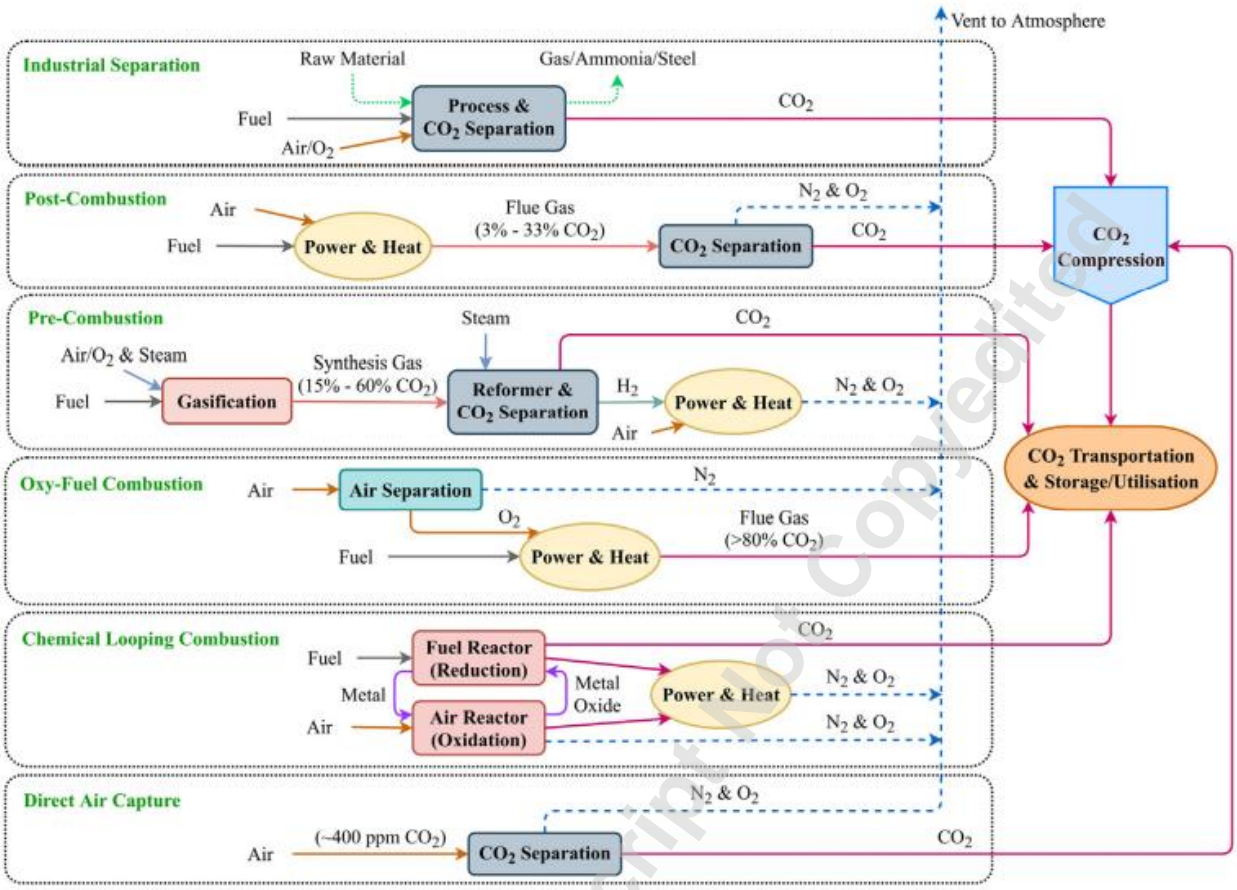


**Fig. 2**. Various carbon capture technologies[12].

Journal of Energy Resources Technology. Received September 16, 2022;
Accepted manuscript posted December 31, 2022. doi:10.1115/1.4056612


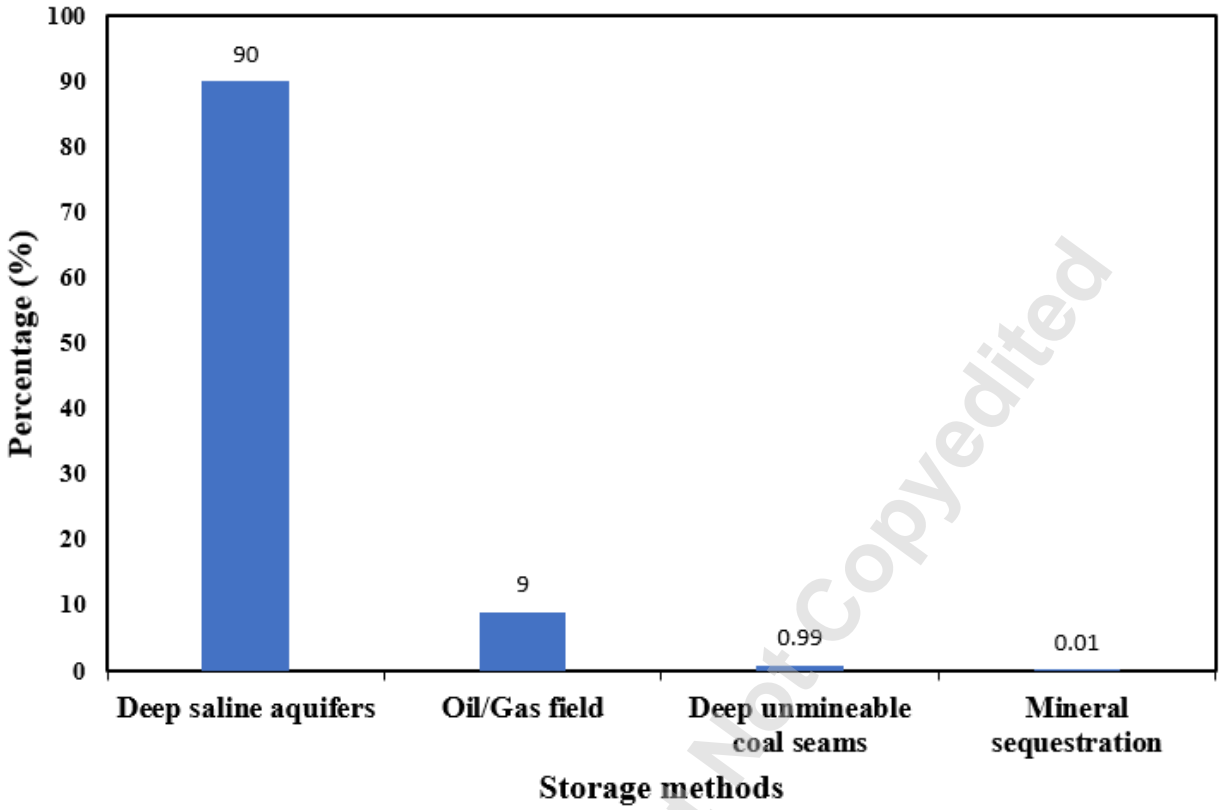


**Fig. 3.** Different magnitude of carbon dioxide storage methods around the World modified from [17].

Table 2: Important characteristics of suitable aquifer for carbon dioxide storage [20].

| | Positive indicators | Cautionary indicators |
|---|---|---|
| Reservoir efficacy | | |
| Static storage capacity | Estimated effective storage capacity much larger than total amount of $CO_2$ to be injected | Estimated effective storage capacity similar to total amount of $CO_2$ to be injected |
| Dynamic storage capacity | Predicted injection-induced pressures well below levels likely to induce geomechanical damage to reservoir or caprock | Injection-induced pressures approach geochemical instability limits |
| Reservoir properties | | |
| Depth | > 1000 m < 2500 m | <800 m > 2500 m |

Journal of Energy Resources Technology. Received September 16, 2022;
Accepted manuscript posted December 31, 2022. doi:10.1115/1.4056612


| | | |
|---|---|---|
| Reservoir thickness (net) | > 50 m | < 20 m |
| Porosity | > 20 % | < 10 % |
| Permeability | > 500 mD | < 200 mD |
| Salinity | > 100 $gl^{-1}$ | > 30 $gl^{-1}$ |
| Stratigraphy | Uniform | Complex lateral variation and complex connectivity of reservoir facies |
| Caprock efficacy | | |
| Lateral continuity | Stratigraphically uniform, small or no faults | |
| Thickness | > 100 m | < 20 m |
| Capillary entry pressure | Much greater than maximum predicted injection induced pressure increase | Similar to maximum predicted injection-induced pressure increase |

Several researchers conducted numerical modeling and simulations on carbon dioxide storage performance and capacity in deep saline aquifers by taking into account various carbon dioxide storage mechanisms combined with other conditions to reflect real-life field life and analyzing some important parameters affecting the storage process. Li et al. [21] analyzed the Ordos basin performance on carbon dioxide storage capacity by considering hysteresis effects. The results revealed that the simulated results at least matched the historical data. Furthermore, Okamoto et al. [22] did a sensitivity analysis on parameters affecting mineralization trapping mechanisms in carbon dioxide storage. It was revealed that reactive surface area and mineral components are important parameters in mineralization trapping mechanisms and might be obtained from laboratory experiments. Zhao et al. [23] conducted a sensitivity analysis on carbon dioxide storage in an aquifer by considering various parameters such as vertical to horizontal permeability ratio, salinity, and residual gas saturation. They did not include hysteresis and mineralization trapping mechanisms. The results revealed that the vertical to horizontal permeability ratio has great effects on carbon dioxide plume movement and amount stored. Lower values of the vertical to horizontal permeability ratio influence more carbon dioxide to dissolve in brine. Kumar et al. [24] did a numerical simulation to quantify most of the trapping mechanisms to store carbon dioxide in a saline aquifer. Three trapping mechanisms were analyzed: residual, solubility, and mineralization trapping mechanisms with the influence of residual gas saturation in the aquifer. Results revealed that residual gas saturation has a great influence on carbon dioxide stored in the aquifer. Further, Orsini et al. [25] conducted numerical modelling and simulation on carbon dioxide storage in an Italian reservoir near the coast. It was found that 69 and 79% of carbon dioxide injected were stored after 1000 and 2000 years, respectively, through a solubility trapping

Journal of Energy Resources Technology. Received September 16, 2022;
Accepted manuscript posted December 31, 2022. doi:10.1115/1.4056612


mechanism. Residual trapping stored 9 and 6% of carbon dioxide injected after 1000 and 2000 years, respectively. Furthermore, the model revealed that 30 Mtons of carbon dioxide will be stored over 20 years of injection with a 38-bar buildup of carbon dioxide injected predicted after stopping injection operation. Khan et al. [26] did a numerical simulation of carbon dioxide storage in an aquifer by considering structural, hysteresis, solubility, and mineralization trapping mechanisms. The results revealed that the hysteresis trapping mechanism is very important in the modeling and simulation of geological carbon dioxide projects. Mo and Akervoll [27] analyzed geological storage capacity of an aquifer to store carbon dioxide by considering residual and solubility trapping mechanisms. The results revealed that solubility trapping mechanisms stored more carbon dioxide and an increase in vertical to horizontal permeability ratio decreased the carbon dioxide trapped. Ozah et al. [28] did numerical simulation on the carbon dioxide storage capacity of an aquifer in three trapping mechanisms: residual, solubility, and mineralization. The results revealed that the mineralization trapping mechanism took a long time to start storing carbon dioxide and stores a lower amount of carbon dioxide gas than the results revealed. However, it is the most stable form in which carbon dioxide is stored. Raza et al. [29] did a numerical simulation by observing the effects of injection rate and calcium carbonate precipitates on structural, residual, and solubility storage trapping mechanisms. The results showed that increasing the injection rate increased the amount of carbon dioxide stored in all trapping mechanisms, both with and without calcium carbonate precipitates. It was added that an optimal rate should be obtained to avoid carbon dioxide leakage risks. Additionally, Akai et al. [30] did numerical simulations on carbon dioxide trapping mechanisms and process activeness by using Sleipner datasets. It was revealed that structural trapping mechanisms dominated during carbon dioxide injection. After injection stopped, residual trapping started to increase. After 100 years of post-injection solubility trapping started to dominate, and after 1000 years of carbon dioxide simulation, mass diffusion in brine became dominant. Al-Khdheeawi et al. [31] analyzed salinity effects on residual and dissolved trapping mechanisms on carbon dioxide storage capacity and plume migration in an aquifer. Results revealed that an increase in salinity decreased carbon dioxide dissolved and trapped. Furthermore, an increase in salinity increases the mobility of carbon dioxide gas. Al-Khdheeawi et al. [32] simulated the impact of water alternating carbon dioxide ($WACO_2$) on different trapping mechanisms such as structural, residual, and solubility on storing carbon dioxide gas. The results revealed that reduction of $WACO_2$ decreased mobility and vertical migration of the carbon dioxide plume. Furthermore, lower $WACO_2$ increases the carbon dioxide stored in solubility and residual trapping mechanisms. Similarly, free gas stored decreased with decreasing $WACO_2$.Raza et al. [33] did a numerical simulation by observing the effects of temperature and precipitation on structural, residual, and solubility storage trapping mechanisms. Temperature increases resulted in an increase in free gas, while residual and dissolved gas decreased with and without precipitation.

Apart from that, Nghiem et al. [34] did numerical modelling and simulation of carbon dioxide sequestration by considering four trapping mechanisms, which are structural trapping mechanisms, residual trapping mechanisms, solubility trapping mechanisms, and mineral trapping mechanisms. Also, they included water injection effects so as to optimize residual and solubility trapping mechanisms. Nghiem et al. [35] conducted simulations on carbon dioxide storage by considering all four trapping mechanisms, water vaporization effects, and thermal effects in their models. However, no study has been conducted that includes four trapping mechanisms, optimization of residual and solubility trapping mechanisms, water vaporization effects, and thermal effects in the modeling and simulation of carbon dioxide storage in deep saline aquifers. Hence, to reflect the real field life, four trapping mechanisms, optimization of residual and

Journal of Energy Resources Technology. Received September 16, 2022;
Accepted manuscript posted December 31, 2022. doi:10.1115/1.4056612


solubility trapping mechanisms, water vaporization effects, and thermal effects have been taken into account during modeling and simulation in low porosity and permeability field in Shenhua CCUS, and this study should be adopted around the world as a reference point for reflecting the reality in carbon dioxide storage projects for areas having the same geological nature and geographical locations. Furthermore, the effects of various key parameters in carbon dioxide storage projects, such as vertical to horizontal permeability ratio, bottomhole pressure, salinity, injection rate, and temperature, on each of the trapping mechanisms have been studied. A part from that carbon dioxide stored in the form of aqueous ions has been reported in this paper.

### *1.1 Carbon dioxide ($CO_2$) storage trapping mechanisms*

There are several active projects around the world that are storing $CO_2$ in geological sites to reduce greenhouse gas emissions, particularly in developed countries. The injected $CO_2$ may be in different phases, such as gas-like, liquid-like, or supercritical. The injected soluble $CO_2$ migrates from the injection well with the local water velocity. It has been researched that $CO_2$ is trapped in four main forms or mechanisms. The physical trapping mechanism that involves carbon dioxide being stored in an anticline that is sealed with caprock (impermeable rock), as shown in Fig. 4(a), is known as structural or stratigraphic trapping mechanisms. In this trapping mechanism, $CO_2$ gas rises above the top after failing to be dissolved and trapped in pore spaces. It is the dominant trapping mechanism [19, 36]. Another $CO_2$ trapping mechanism is the residual trapping mechanism, which is also a physical $CO_2$ trapping mechanism that depends on the movement of $CO_2$ and aqueous phase through hysteresis/capillary forces in which carbon dioxide is trapped and stored in pore spaces after displacing the wetting phase (brine) and then the displaced brine fluid returns to pore spaces to seal the $CO_2$ trapped and become immobile as shown in Fig. 4 (b).A residual trapping mechanism has been reported as the fastest trapping mechanism with time[37-39]. Also, solubility trapping, which is a chemical $CO_2$ trapping mechanism which stores $CO_2$ as a soluble component in brine. In this trapping mechanism, carbon dioxide is injected dissolved in brine to form a higher density and more stable fluid than brine, as shown in Fig. 4 (c)[40, 41]. Lastly, is the mineral trapping mechanism, which is a geochemical trapping $CO_2$ mechanism in which $CO_2$ dissolves in brine and surrounding rocks and precipitates to form minerals Fig. 4 (d). $CO_2$ is converted into carbonate minerals like calcite, dolomite, siderite, etc. This carbon dioxide storage mechanisms take hundreds to thousands of years to be observed [19, 39, 42-44]. The different $CO_2$ trapping mechanisms evolutions to store carbon dioxide depends highly on the local conditions of a particular area. To estimate storage capacity of each trapping mechanisms depends on the time scale at which mechanisms evolved (become active)[11]. Estimated evolution time scale of different $CO_2$ trapping mechanisms in a deep saline aquifer is shown in Fig. 5.

Journal of Energy Resources Technology. Received September 16, 2022;
Accepted manuscript posted December 31, 2022. doi:10.1115/1.4056612


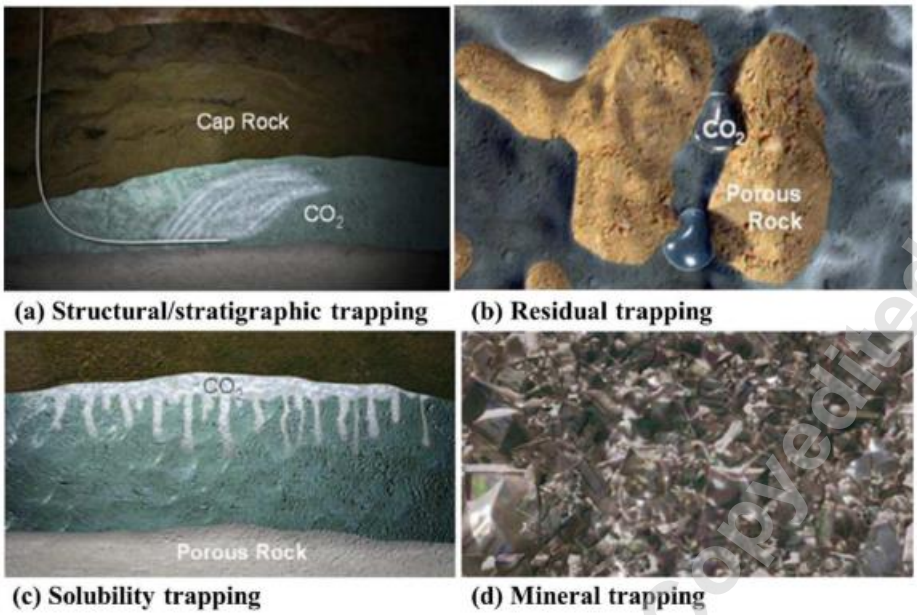


**Fig. 4** Carbon dioxide trapping mechanisms[45].

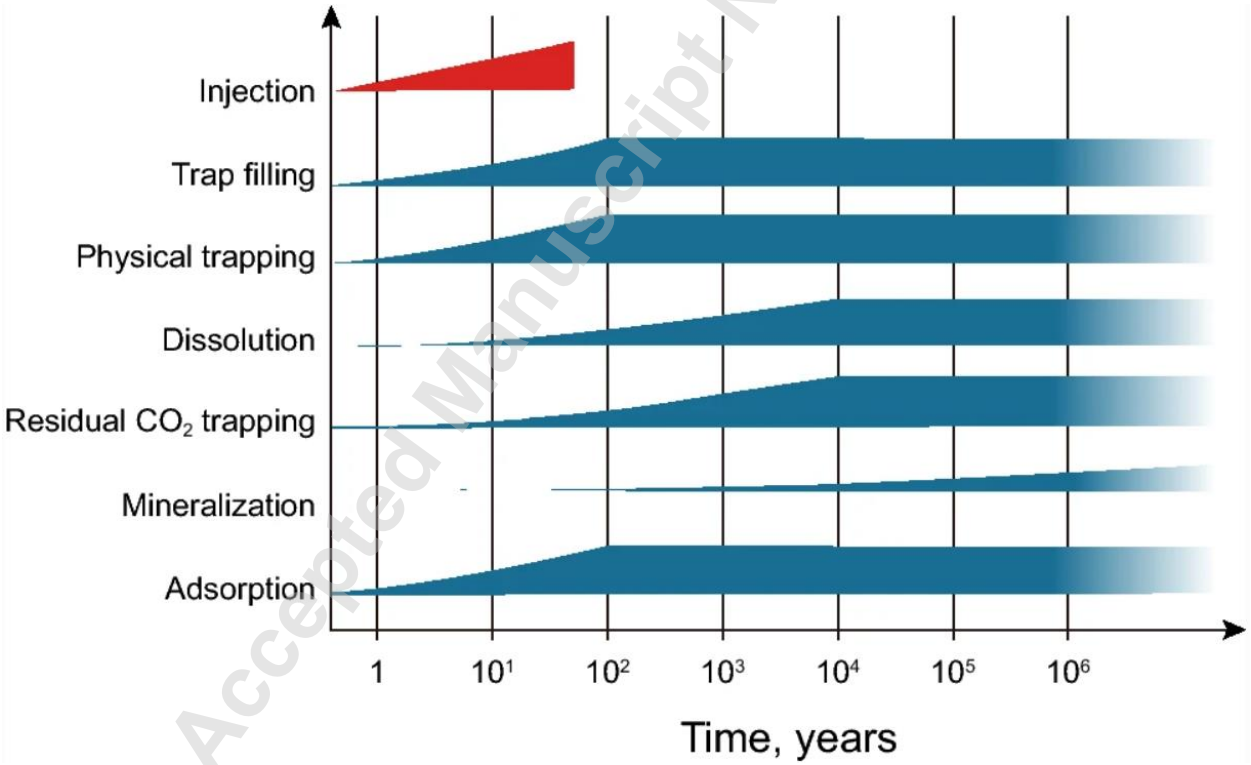


**Fig.5** Time at which different carbon dioxide trapping mechanism come into effects during injection and post injection[11, 46].

Journal of Energy Resources Technology. Received September 16, 2022;
Accepted manuscript posted December 31, 2022. doi:10.1115/1.4056612


*1.2 Uncertainty of $CO_2$ trapping mechanisms*

There are several uncertainties about $CO_2$ trapping mechanisms during $CO_2$ storage. In structural trapping mechanisms, the possible uncertainty is the high risk of leakage if the caprock fails because $CO_2$ is stored as free gas. In a residual gas trapping mechanism, the leakage risk is low because $CO_2$ is stored in pore spaces. In the solubility trapping mechanism, the leakage risk is low because $CO_2$ is dissolved in brine to form a soluble component. However, in this trapping mechanisms, there is a high risk of $CO_2$ migration. In a mineral trapping mechanism, the leakage risk is very low because $CO_2$ reacts with pore water and rocks to form carbonate minerals. This is the safest storage process, but it moves very slowly compared to others and is more uncertain in prediction. These four trapping mechanisms for storage security are shown in Fig. 6[39].

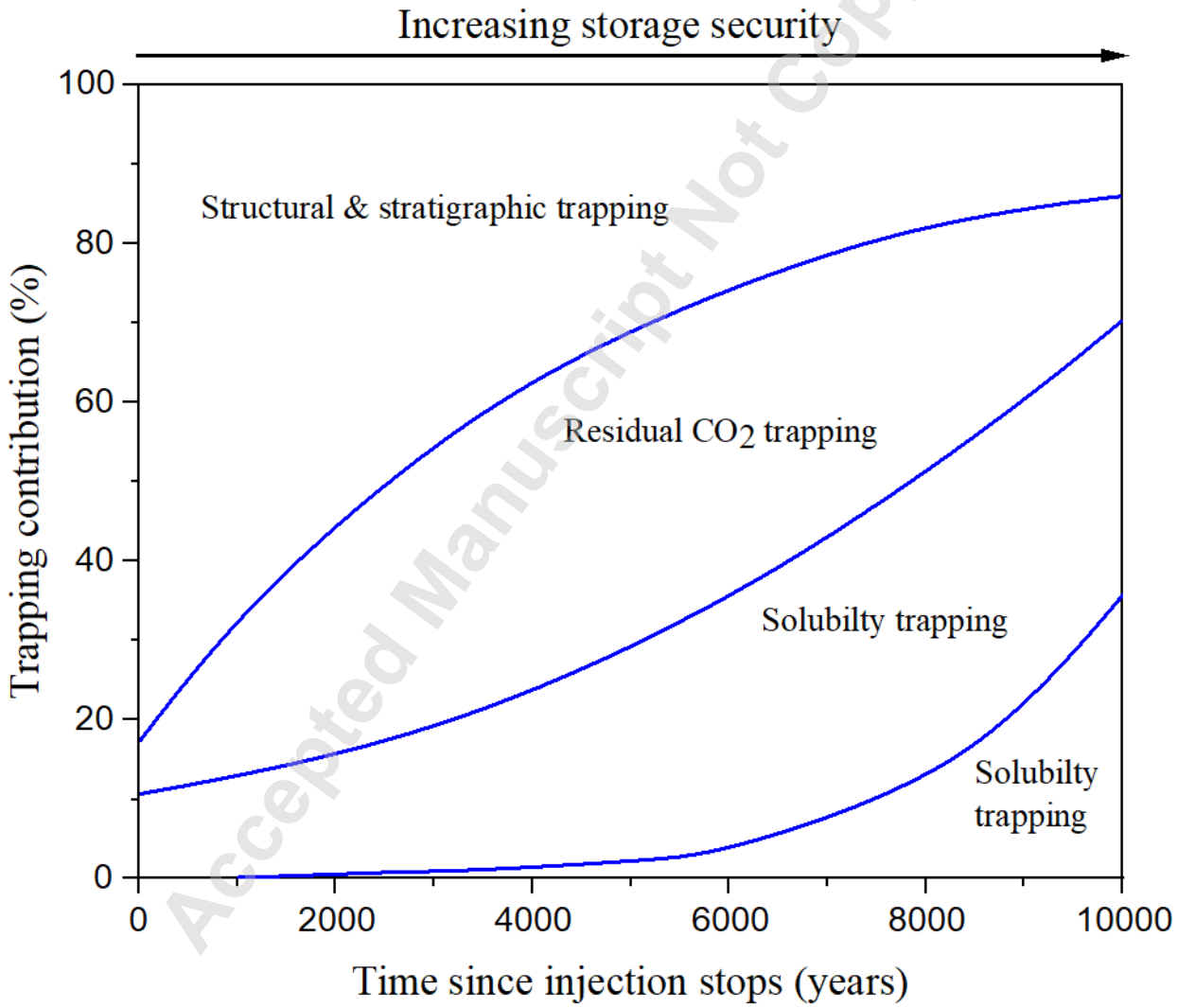


**Fig. 6** Carbon dioxide trapping mechanisms storage stability modified from [34, 47].

Journal of Energy Resources Technology. Received September 16, 2022;
Accepted manuscript posted December 31, 2022. doi:10.1115/1.4056612


## 2. Methodology

### *2.1 Case study*

China is in the initial stages of carbon storage. However, they have developed carbon capture technology[48]. The Shenhua deep saline aquifer is one of the main and most promising Chinese aquifer projects launched in May 2011. This project is a guideline for all future projects that will be constructed in the same area [48, 49]. As shown in Fig. 7(a), the Shenhua carbon capture and storage (CCS) facility is located in the eastern part of the Ordos basin, north of the Yishan slope. It is a special area isolated for geological carbon storage in China. It is characterized by Triassic and Permian sandstone formations with a deep saline aquifer. The Shenhua deep saline aquifer has five reservoir formations which are Shanxi, Liujiagou, Shihezi, Majiagou, and Shiqianfeng with a sedimentary thickness of 1500 m from the Ordovician to Lower Triassic era [50, 51]. It has low porosity and permeability, which means slow groundwater movement. The slow ground movement made it ideal for carbon dioxide storage[52]. The permeability ranges from 0.02 to 6.8 mD and the porosity ranges from 6 to 12.9% after core sample analysis. Because their target is to store approximately 100,000 metric tons per year, low porosity and permeability were not favorable. This made them to fracture the formation so as to meet injection target. The stratigraphic column is shown in Fig. 7 (b).

Journal of Energy Resources Technology. Received September 16, 2022;
Accepted manuscript posted December 31, 2022. doi:10.1115/1.4056612


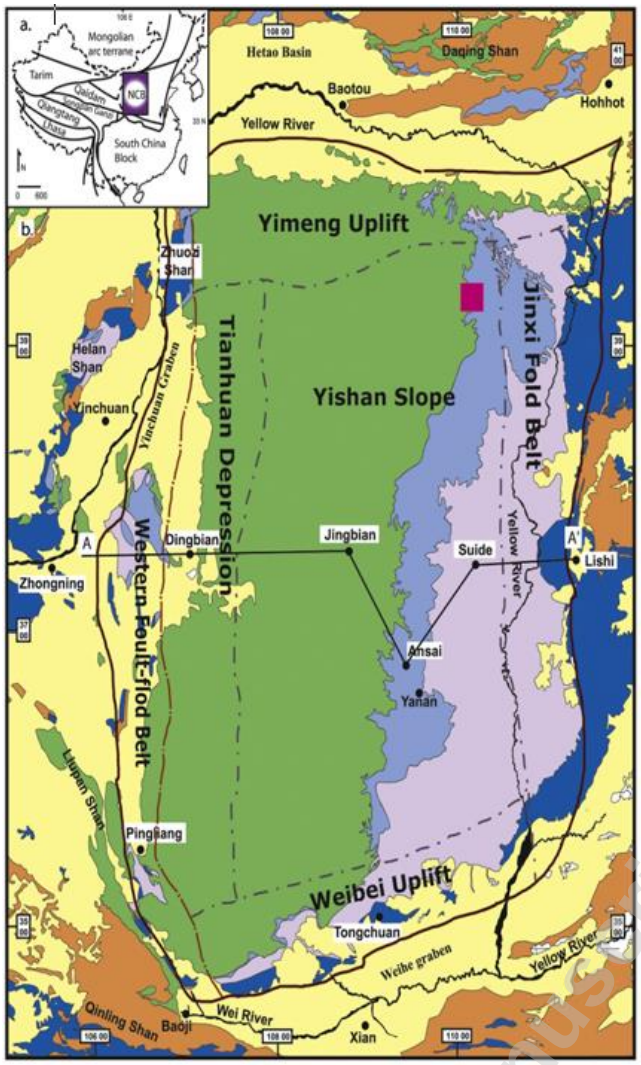


a)

| Stratum | | | Group | | Thickness (m) |
|---|---|---|---|---|---|
| Period | System | Series | | | |
| Cenozoic | Quaternary | | | | 0-30 |
| Mesozoic | Cretaceous | | Luohe | | 0-137 |
| | Jurassic | Middle | Anding | | 80-150 |
| | | | Zhiluo | | 200-400 |
| | | Lower | Yanan | | 250-300 |
| | Triassic | Upper | Yanchang | | 790-1415 |
| | | Middle | Zhifang | | 300-530 |
| | | Lower | Heshanggou | | 47-169 |
| | | | Liujiagou | Upper | 202-422 |
| | | | | Middle | |
| | | | | Lower | |
| Upper Paleozoic | Permian | Upper | Shiqianfang | Upper | 200-345 |
| | | | | Lower | |
| | | | Shihezi | Upper | 200-340 |
| | | Lower | | Lower | 80-200 |
| | | | Shanxi | | 37-125 |
| | Carboniferous | | Taiyuan | | 22-276 |
| | | | Benxi | | 15-58 |
| Lower Paleozoic | Ordovician | Lower | Majiagou | | 100-100 |

b)

Fig. 7 Modified a) Field location of Shenhua deep saline aquifer marked with red box b) Stratigraphic column of Ordos basin[53].

*2.2 Model description and set up*

A 3D homogeneous carbon dioxide sequestration model with a total grid block of 1,000,000 with a dimension of 100 ×50×20 in x, y and z directions was built in by using the input data as shown in Table 3. Fig. 8 shows the 3D aquifer base case model. 2D porosity and permeability distributions are shown in Figs. 9 (a) and (b), respectively. In this study, a commercial reservoir simulator software, computer modelling group CMG 2021 version, was used to build and simulate the model. Builder, CMG-GEM, and Winprop were used. Builder was used to build a model. Winprop was used to build a compositional fluid model as an input for GEM. The data used to build the compositional fluid model in Winprop is shown in Table 4. GEM was used to simulate the whole model. GEM, which is a compositional, chemical, and unconventional leading equation of state reservoir simulation modelling software, GEM has integrated equations which

Journal of Energy Resources Technology. Received September 16, 2022;
Accepted manuscript posted December 31, 2022. doi:10.1115/1.4056612


enable us to model and simulate carbon dioxide flow and storage in the reservoir as well as enhance oil recovery processes, especially secondary and tertiary oil recovery techniques. It handles the miscible and immiscible injection processes, including physical and chemical reactions of multiple component systems [16, 54-56].

Table 3 Input data used to build the model.

| Name of parameter | Value |
|---|---|
| Reservoir grid dimensions | 100 ×50×20 |
| Reservoir permeability | 0.02 to 6.8 mD |
| Reservoir porosity | 6 to 12.9% |
| Reservoir temperature | 56.03 to 63.83 $^{\circ}$C |
| Injection temperature | 50 $^{\circ}$C |
| Salinity | 0.1% =100000ppm |
| Rock compressibility | $4.5 \times 10^{-10}$ 1/kPa |
| Rock density | 2600 kg/m$^3$ |
| Reference depth | 1699 to 1990 m |
| Thickness | 123 m |
| Dip angle | 0 |

Table 4 Compositional fluid model data inputs

| No. | Component | Mole fraction | $P_C$ (atm) | $T_C$(K) | Acentric factor | MW | SG |
|---|---|---|---|---|---|---|---|
| 1 | $CO_2$ | 3 | 72.8 | 304.2 | 0.225 | 44.01 | 0.818 |
| 2 | $CH_4$ | 1 | 45.4 | 190.6 | 0.008 | 16.043 | 0.3 |
| 3 | $H_2O$ | 2 | 217.6 | 647.3 | 0.344 | 18.015 | 1 |

Journal of Energy Resources Technology. Received September 16, 2022;
Accepted manuscript posted December 31, 2022. doi:10.1115/1.4056612


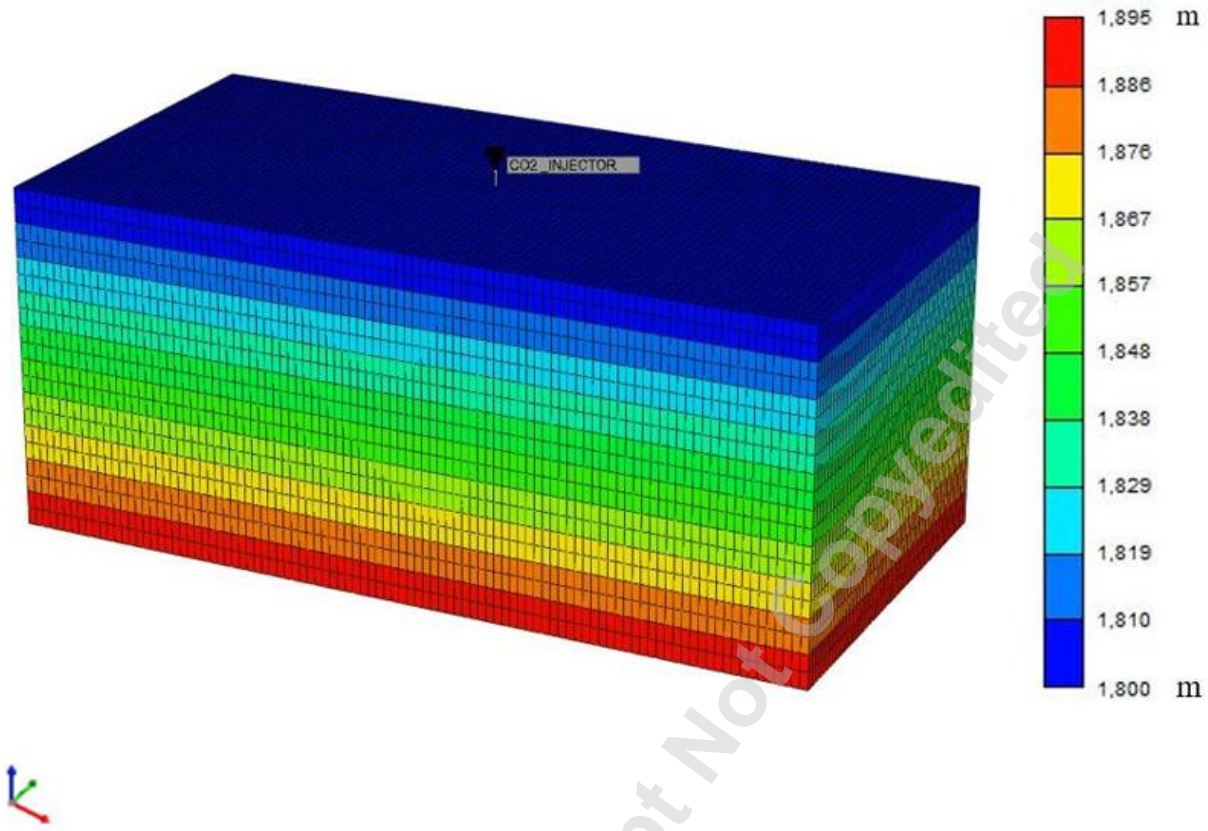


Fig. 8 3D $CO_2$ sequestration grid base case model.

a)

Journal of Energy Resources Technology. Received September 16, 2022;
Accepted manuscript posted December 31, 2022. doi:10.1115/1.4056612


b)

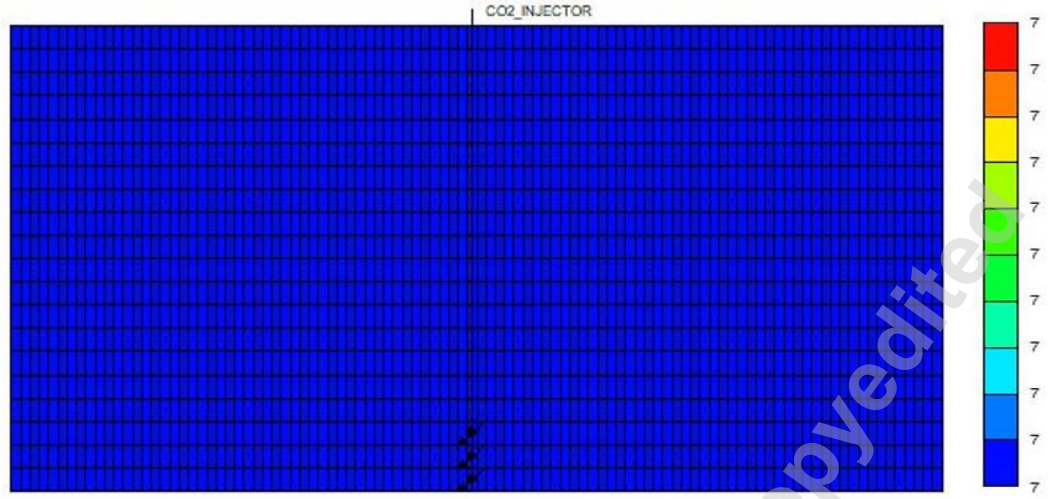


Fig. 9 a) Porosity distribution (fraction) b) Permeability distribution (mD)

Rock and relative permeability data are very important in building and simulating the model. Water-gas relative permeability data in the modeling of carbon dioxide storage helps with guiding fluid movements in the reservoir. Because the wellbore is surrounded by water, relative permeability helps in easing the injection process. In this paper, gas water-gas relative permeability curves were estimated by using Corey [57] correlations as shown in Fig .10. In this study, the injector well was located at the middle of the reservoir with perforation located at (50,25,16-20) in x, y, and z directions. The carbon dioxide gas was injected at a maximum injection rate of 10,000 $m^3$/day with a maximum bottom hole pressure of 44,500 kPa at standard temperature and pressure. The gas was injected in a supercritical state for 15 years, followed by 833 years of post-injection. The water injector well was located 100m above the carbon dioxide injector well.

Journal of Energy Resources Technology. Received September 16, 2022;
Accepted manuscript posted December 31, 2022. doi:10.1115/1.4056612


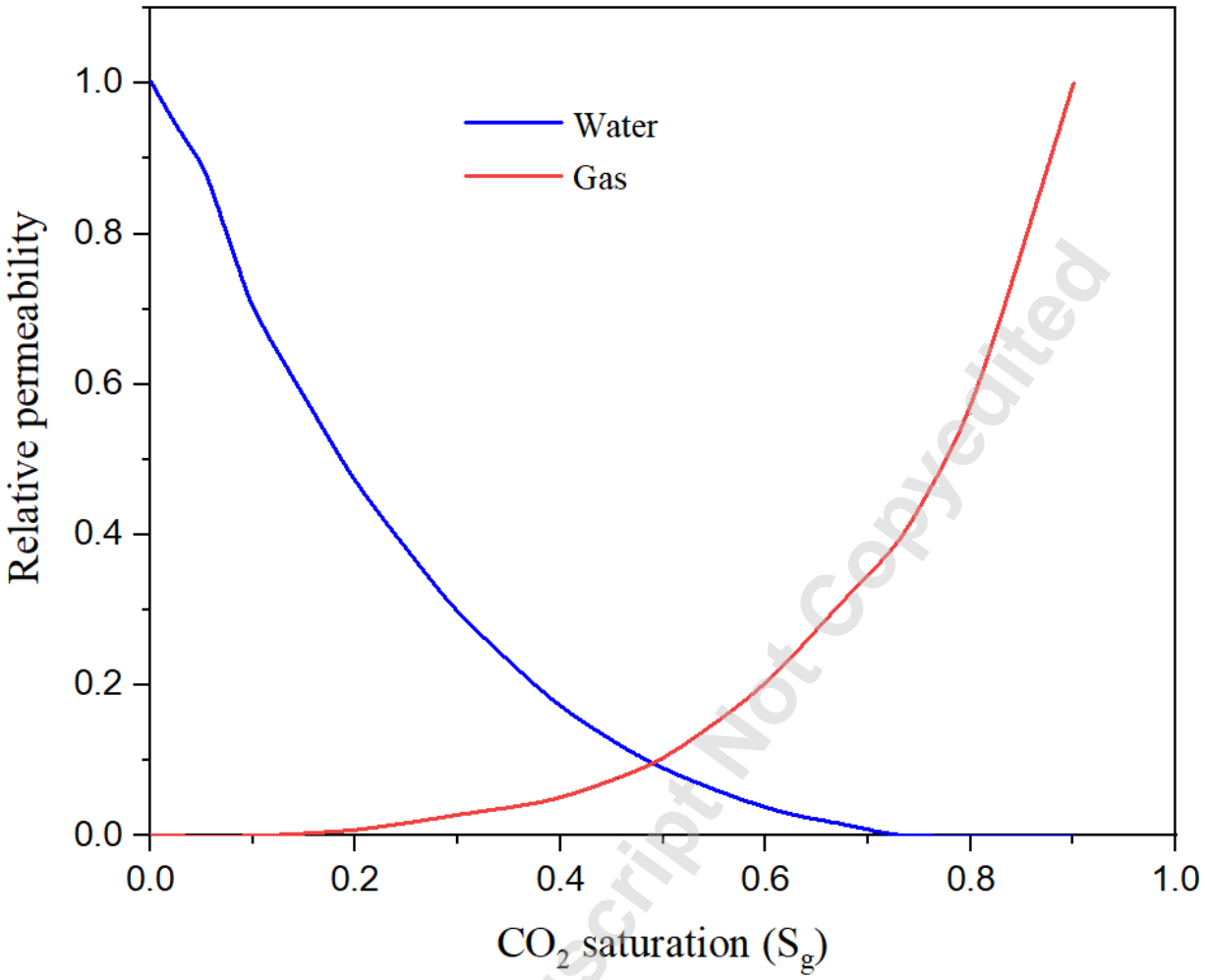


Fig. 10 Water-gas relative permeability curve.



*2.3 Governing equations*

*2.3.1 Equation of state (EOS)*

EOS is used in compositional reservoir simulations. EOS is an accurate and powerful means to model complicated phase and flow behaviors common in the displacement of oil and gas in petroleum reservoirs. CMG-GEM adopted this idea for CO2 sequestration modelling. The advantage of the EOS expression over other oil and gas PVT models is that it combines simple expressions for thermodynamic properties and phase equilibrium relationships of interest with high accuracy in prediction. Mass and momentum conservation equations govern the entire process of modeling and simulating carbon dioxide transport and multiphase flow in porous media. Darcy's

laws, which integrate mass and momentum conservation, have been employed to model and simulate the carbon dioxide storage in an aquifer. Darcy's law is depicted in Eq. 1 as a partial differential equation[16, 58, 59].

$$\frac{\partial M^K}{\partial t} = -\nabla . F^K + q^K \tag{1}$$

Where M, F, K stands for mass buildup in Kg/m$^3$, F is mass flux in kg/m$^2$s, and q is source or sink in kg/m$^3$s.

In aquifer which contain water component the Eq. 1 can be expressed in form of Eq. 2.

$$\frac{\partial}{\partial t}\left[\phi\left(X_l^w S_l \rho_l + X_g^w S_g \rho_g\right)\right] = -\nabla .\left\{X_l^w \rho_l\left(-k\frac{k_{rl}}{\mu_l}\left(\nabla P_l - \rho_l g\right)\right) + X_g^w \rho_g\left(-k\frac{k_{rg}}{\mu_g}\left(\nabla P_g - \rho_g g\right)\right)\right\} + \left(q_l^w + q_g^w\right)$$

(2)

Where $\phi$ is porosity, $X_l^w$ is mass fraction of component w in liquid phase, S is saturation of liquid phase, k is permeability is pressure, w stands for water, ρ is density, g stands for gas, $k_{rg}$ is relative permeability of gas, μ is viscosity.

Then the governing equations for carbon dioxide multiphase flow component system is written as:

$$\frac{\partial}{\partial t}\left[\phi\left(X_l^C S_l \rho_l + X_g^C S_g \rho_g\right)\right] = -\nabla .\left\{X_l^C \rho_l\left(-k\frac{k_{rl}}{\mu_l}\left(\nabla P_l - \rho_l g\right)\right) + X_g^C \rho_g\left(-k\frac{k_{rg}}{\mu_g}\left(\nabla P_g - \rho_g g\right)\right)\right\} + \left(q_l^C + q_g^C + q_s^C\right)$$

(3)

Here C stands for carbon dioxide.

### *2.3.2 Hysteresis effects modeling*

Hysteresis effects is very important to be taken into account during carbon dioxide modelling and simulation. It takes into account the wettability and capillary effects of an immobile trapped gas into pore spaces [34] . There are several established models established to take into account this residual gas trapped in pore spaces[60].The Land model was used to model two-phase hysteresis effects in this paper. Hysteresis effects are illustrated in the relative permeability curve in Fig. 11. From the figures, it shows that the gas relative permeability trails the drainage curve (black colored) when gas saturation increases. When gas saturation reverses its course (decreases), for

Journal of Energy Resources Technology. Received September 16, 2022;
Accepted manuscript posted December 31, 2022. doi:10.1115/1.4056612


instance at point $S_{gi}^{*}$ at drainage curve, then the relative permeability curve trails the imbibition curve (red curve). The residual gas saturation for a certain gas saturation ($S_{gi}^{*}$) is given in Eq. 4 [24, 61].

$$S_{gt}^{*}\left(S_{gi}^{*}\right)=\frac{S_{gi}^{*}}{1+CS_{gi}^{*}} \tag{4}$$

The lands model coefficient is given by Eq. 5.

$$C=\frac{1}{S_{gt,\max}}-\frac{1}{S_{g,\max}} \tag{5}$$

Where $S_{gt,max}$ and $S_{g,max}$ represent maximum trapped gas saturation and maximum gas saturation that should be reached.

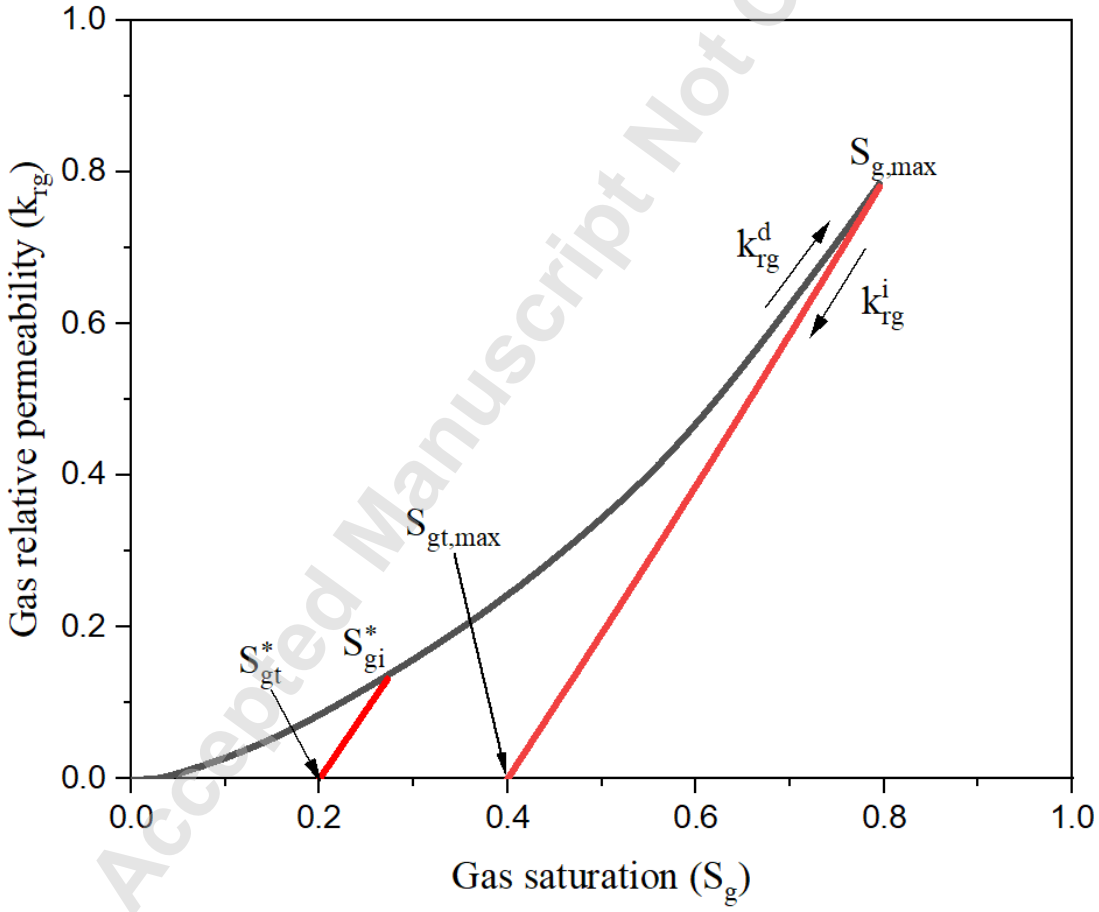


Fig. 11 Lands model gas relative permeability curve ,redrawn from [34].

Journal of Energy Resources Technology. Received September 16, 2022;
Accepted manuscript posted December 31, 2022. doi:10.1115/1.4056612


*2.3.3 $CO_2$ solubility modeling in brine*

Carbon dioxide solubility depends on pressure, temperature, surface area and contact area with brine. The solubility of carbon dioxide in the brine is modeled by different equation of state (EOS) models [62]. In this paper, Peng-Robinson EOS was used to estimate pressure, density, and temperature of reservoir fluids and brine density, carbon dioxide solubility, and brine viscosity [63]. Because the dissolution rate is very fast, the carbon dioxide gas and brine are assumed to be in thermodynamic equilibrium. The equation for thermodynamic equilibrium is the equality of fugacities [16, 64]:

$$g_i = f_{ig} - f_{iw} = 0, i = 1, 2...., n_g, \quad (6)$$

Where $f_{ig}$ is fugacity of component i in the gas phase ($CO_2$) which is calculated from Peng-Robinson EOS, $f_{iw}$ is fugacity of component i in the aqueous phase (brine) which is calculated by using Henrys law that establishes the proportionality of components fugacity to its concentration:

$$f_i = x_i * H_i \quad (7)$$

Where $x_i$ is concentration and $H_i$ is Henry constant. Henry constant is a function of pressure, temperature and salinity. So, the increase in pressure causes the solubility to increase whereas increase in temperature and salinity causes decrease in solubility(reference).

*2.3.4 Mineralization modeling in $CO_2$ sequestration*

Fast reversible aqueous reactions are modeled with chemical equilibrium reactions. The governing equation is the equality between activity products and chemical equilibrium constant (Keq) as expressed in Eqs. 8 and 9. The rate law for mineral dissolution and precipitation is governed by a mineral reaction rate model known as the Transition State Theory (TST) model, as illustrated in Eq. 10 [65-70].

$$K_{eq}(T) = \frac{a_{H^+}.a_{HCO_3^-}}{a_{CO_{2(aq)}}.a_{H_2O}} \quad (8)$$

Where a is activity which is also a measure of concentration.

$$r_\beta = \hat{A}_\beta k_\beta \left(1 - \frac{Q_\beta}{K_{eq,\beta}}\right), \beta = 1,2, \dots, R_{mn} \quad (9)$$

And

$$\hat{A}_j = \hat{A}_j^0 . \frac{N_j}{N_j^0} \quad (10)$$

Where Q is activity product, $K_{eq}$ is mineral chemical equilibrium constant, A is mineral reactive surface area, $Q/K_{eq}$ is saturation index which controls the direction of the mineral reaction, when

is greater than one means precipitation and less than one means dissolution, and K is rate constant of the mineral reaction[65-70].Rate constant of the mineral reaction is a function temperature as expressed in Eq. 11. The rate constants of reaction are usually reported in the literature at a reference temperature (298.15K or 25°C)[65-70].

$$k = k_0 \exp\left[-\frac{E_a}{R}\left(\frac{1}{T}-\frac{1}{T_0}\right)\right] \tag{11}$$

Where k is reaction rate at a certain temperature, $k_0$ is reference temperature reaction rate, E is mineral reaction activation energy, and R is universal gas constant[65-70].In this paper the GEM-GHG aqueous reactions and mineral species used are shown in Tables 5 and 6.

Table 5 GEM-GHG aqueous reaction selected

| Aqueous species reactions |
|---|
| $CO_{2(aq)} + H_2O = H^+ + HCO_3^-$ |
| $HCO_3^- + H^+ = HCO_3^-$ |
| $OH^- + H^+ = H_2O$ |

Table 6 GEM-GHG mineral species reaction selected

| Mineral reactions | Reactive surface areas | $Log_{10}$(Rate constant) at Tref | Activation energy | Reference temperature |
|---|---|---|---|---|
| Unit | $m^2/m^3$ | $mol/m^2s$ | J/mol | deg C |
| Anorthite $+8.0\ H^+ = 4.0\ H_2O + Ca^{++} + 2.0\ Al^{+++}$ | 88 | -12 | 67830 | 25 |
| Kaolinite $+ 6.0\ H^+ = 5.0\ H_2O + 2.0\ Al^{+++} + 2.0\ SiO_{2(aq)}$ | 88 | -8.79588 | 41870 | 25 |
| Calcite $+ H^+ = Ca^{++} + HCO_3^-$ | 17600 | -13 | 62760 | 25 |

*2.3.5 Water vaporization effects during gas injection*

Zuluaga and Lake [71] expressed how to model vaporization effects during gas injection. It was reported that vaporization depends on temperature and pressure and that it increases as temperature increases with a decrease in pressure. The higher pressure drop and increase in temperature with depth cause water vaporization near the wellbore, which leads to salt precipitation, which in turn causes a reduction in porosity and permeability [72, 73]. To take into account water vaporization effects, which occur during gas injection and that in turn affect the gas injectivity around the wellbore. Thermodynamic equilibrium to water component application is modelled and considered by Eq. 12 in this study.

$$f_{H_2O,g} = f_{H_2O,aq} \tag{12}$$

Where $\mathbf{f_{H_2O,g}}$ is calculated from cubic EOS and $\mathbf{f_{H_2O,aq}}$ is calculated by Eq. 13.

$$f_{H_2O,aq} = y_{H_2O,aq} \cdot f_{H_2O,aq} \tag{13}$$

$$f_{H_2O} = f^S_{H_2O} . \exp\left( \int_{p^S_{H_2O}}^{p} \frac{v_{H_2O}}{RT} dp \right) \tag{14}$$

Where $f^S_{H_2O}$ is fugacity of water at saturation pressure and temperature and $p^S_{H_2O}$ is saturation pressure of water.

*2.3.6 Modeling temperature effects*

When carbon dioxide is injected into the deep saline aquifer, it cools lower than the formation temperature even if it is heated at the surface, due to Joule-Thomson cooling effects. Furthermore, water vaporization effects around the wellbore may cause the temperature of carbon dioxide to drop from 1 to $2^0$C[74]. The temperature difference between injected carbon dioxide and surrounding rocks can cause casing failure. In addition to that, this temperature difference between injected carbon dioxide and the formation can cause thermal stress changes to the surrounding rocks, which may induce fissures or fractures in the caprocks that may lead to carbon dioxide leakage. Furthermore, if there is a cycling injection and shut-in process in the storage site, cooling and heating of surrounding rocks and casing can occur, and this may cause carbon dioxide leakages through caprock, casing, and abandoned wells [75, 76]. To take into account thermal effects is modeled by using Eq. 16 [35].

$$\Delta T_g H_g \Delta\Phi_g + \Delta T_{aq} H_{aq} \Delta\Phi_{aq} + \Delta\tau_c \Delta T + Q_{loss} + \sum_k H_k q_k - \frac{V}{\Delta t}\left[ \phi^{n+1}\left( \sum_k \rho_k^{n+1} S_k^{n+1} U_k^{n+1} \right) - \phi^n \left( \sum_k \rho_k^n S_k^n U_k^n \right) \right] - \frac{V}{\Delta t}\left[ \left(1-\phi^{n+1}\right)_{C_R \tilde{\rho}_R} \left( T^{n+1} - T_R^0 \right) - \left(1-\phi^{n+1}\right)_{C_R \tilde{\rho}_R} \left( T^n - T_R^0 \right) \right] = 0, k = g, aq \tag{16}$$

Where T represents temperature, H is Henry law constant, $\Phi$ is potential, $\tau$ stands for the total thermal conductivity , $Q_{loss}$ is heat loss, $q$ is rate, V is grid block volume, $\Delta t$ is change in time, $\phi$ is porosity, ρ represent density, $S$ is saturation, $U$ is molar internal energy .For subscripts g represents gas, *aq* stands for aqueous phase, c is rocks and fluids, k is phase, C is Lands coefficient ,R is universal gas constant, $\tilde{\rho}$ is mass density.

Journal of Energy Resources Technology. Received September 16, 2022;
Accepted manuscript posted December 31, 2022. doi:10.1115/1.4056612


*2.3.7 Acceleration of residual and solubility trapping mechanisms*

Residual gas and solubility trapping mechanisms are the two most important carbon dioxide storage trapping mechanisms because carbon dioxide is stored in an immobile phase in pore spaces and as a solution in brine, respectively. It has been reported that water injection or water alternating gas (WAG) during carbon dioxide sequestration accelerates residual and solubility trapping mechanisms due to hysteresis effects and dissolution effects. For lower permeability aquifers, it is recommended to add water injector above carbon dioxide injector, whereas for higher permeability aquifers, it is recommended to add water injector separately with carbon dioxide injector [43]. The mechanism behind this process is that when water is injected with carbon dioxide, carbon dioxide moves upward and water moves down after forming a water-carbon mixture in an aquifer. This accelerates more carbon dioxide to be trapped and dissolved in water [43, 77].In the case of WAG operation, it is recommended that the mobility ratio should be kept at less than one in order to control carbon dioxide plume migration and avoid viscous fingering effects. Also, when the mobility ratio is less than one, it reduces upward migration of carbon dioxide gas and increases carbon dioxide dissolution, which in turn increases carbon dioxide trapped in pore spaces and dissolved in brine. Mobility ratio is the ratio of the mobility of non-wetting fluid to the mobility of wetting fluid, expressed as a in Eq. 17 [78-80].

$$M = \frac{\lambda_w}{\lambda_{CO_2}} = \frac{\mu_w / k_{rw}}{\mu_{CO_2} / k_{rCO_2}} = \frac{\mu_w . k_{rCO_2}}{\mu_{CO_2} . k_{rw}} \tag{17}$$

Where $\lambda_w$ and $\lambda_{CO_2}$ are mobility of water and carbon dioxide, $\mu_w$ and $k_{rw}$ are viscosity and relative permeability of water, $\mu_{CO_2}$ and $k_{rCO_2}$ are viscosity and relative permeability of carbon dioxide, respectively.

## 3. Results and discussions

During 15 years of injection, most of the injected carbon dioxide gas is stored as free gas, which migrates to the top of the aquifer (Fig. 12a) due to buoyancy effects and the density difference between pure carbon dioxide and dissolved carbon dioxide in the brine which falls down the aquifer. After stopping injection, the pressure difference exists between the top of the aquifer and other areas, and this pressure difference causes the free gas to fall down and start to migrate horizontally and get dissolved in brine, trapped in pore spaces, with others stored in mineral form. As the post injection period increases, the carbon dioxide plumes continue to migrate horizontally as shown in Fig. 12 (b-d).

Journal of Energy Resources Technology. Received September 16, 2022;
Accepted manuscript posted December 31, 2022. doi:10.1115/1.4056612


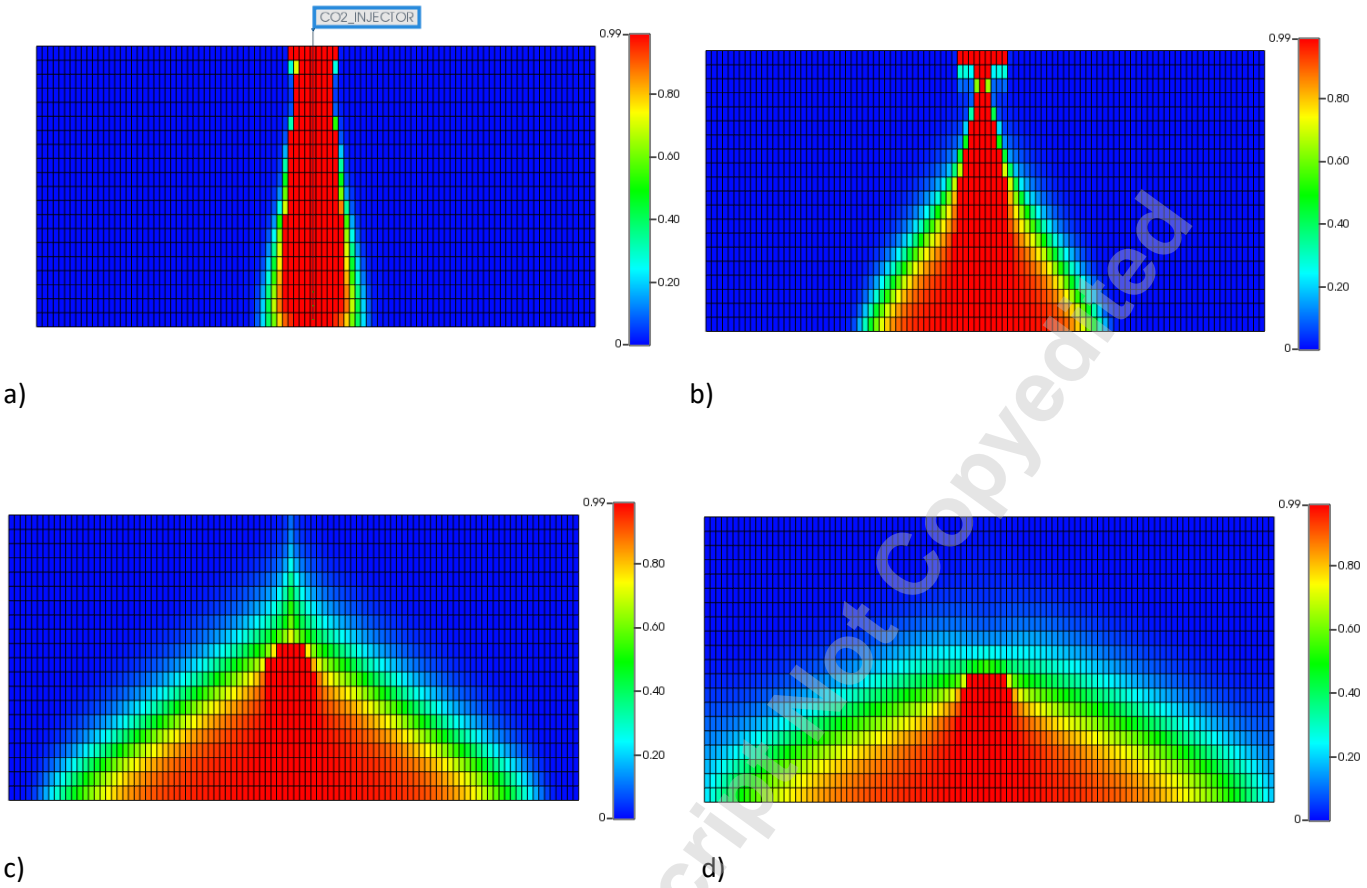


Fig. 12 Carbon dioxide mole fraction distribution a) During 15 years of injection b)100 years of post-injection c)500 years of post-injection d) 833 years of post-injection.

### *3.1 $CO_2$ stored in different forms of trapping mechanisms*

After 15 years of carbon dioxide injection and 833 of post injection, the carbon dioxide gas storage capacity for different carbon dioxide storage trapping mechanisms is shown in Fig. 13. It shows that supercritical and trapped carbon dioxide reach their maximum during injection and then start to decrease in post injection process, whereas aqueous, mineral, and dissolved carbon dioxide increase slowly from the start of injection to the post injection process. The cumulative carbon dioxide stored during 15 years of injection and 833 of post injection for different forms of carbon dioxide storage mechanisms is shown in Tables 6 and 7, respectively. During the first 15 years of carbon dioxide injection, supercritical accounts for 58.35% of the carbon dioxide injected, followed by trapped 29.79%, dissolved 10.25%, aqueous ions 1.46%, and 0.15% mineral forms.

Journal of Energy Resources Technology. Received September 16, 2022;
Accepted manuscript posted December 31, 2022. doi:10.1115/1.4056612


During post injection, most carbon dioxide was stored in a supercritical state by 33.3%, followed by dissolved 32.2%, trapped 31.05%, aqueous 2.01%, and 1.44% mineral forms.

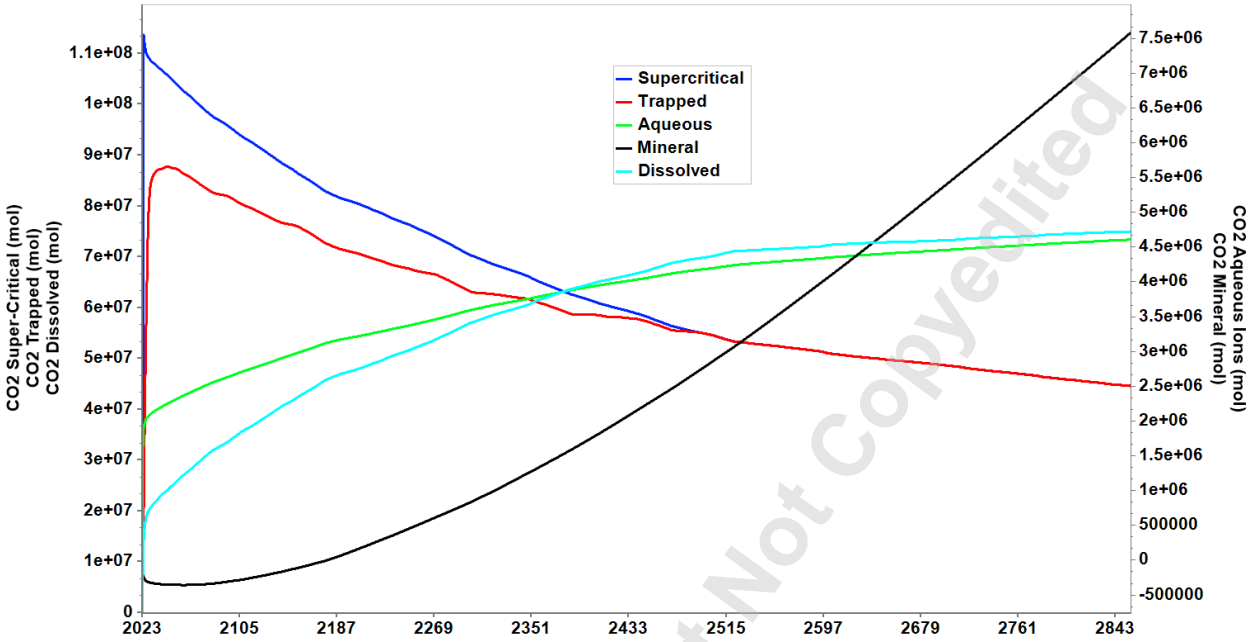


Fig.13 $CO_2$ stored in different forms of trapping mechanisms.

Table 6 Field cumulative carbon dioxide injection after 15 years of injection

| Supercritical $CO_2$ ($\times 10^{10}$) (mol) | Trapped $CO_2$ ($\times 10^{10}$) (mol) | Dissolved $CO_2$ ($\times 10^{9}$) (mol) | Aqueous $CO_2$ ($\times 10^{9}$) (mol) | Mineral $CO_2$ ($\times 10^{8}$) (mol) | Total $CO_2$ ($\times 10^{10}$) (mol) |
|---|---|---|---|---|---|
| 4.093 | 2.090 | 7.187 | 1.024 | -1.099 | 7.015 |

Negative (-) sign show that $CO_2$ injected were dissolved in brine and rock surface before precipitating to form minerals.

Table 7 Field cumulative carbon dioxide injection after 833 years of post-injection

| Supercritical $CO_2$ ($\times 10^{11}$) (mol) | Trapped $CO_2$ ($\times 10^{11}$) (mol) | Dissolved $CO_2$ ($\times 10^{11}$) (mol) | Aqueous $CO_2$ ($\times 10^{10}$) (mol) | Mineral $CO_2$ ($\times 10^{10}$) (mol) | Total $CO_2$ ($\times 10^{12}$) (mol) |
|---|---|---|---|---|---|
| 6.29 | 5.866 | 6.082 | 3.778 | 2.72 | 1.889 |

Journal of Energy Resources Technology. Received September 16, 2022;
Accepted manuscript posted December 31, 2022. doi:10.1115/1.4056612


### *3.2 Effects of injection rate in $CO_2$ sequestration*

The carbon dioxide injection rate is very important in determining the amount and efficiency of geological sites to store carbon dioxide. Injection rate is controlled by injection pressure and must be controlled not to reach maximum pressure buildup, which can cause damage and leakage of cap rock that may lead to the escape of carbon dioxide to the atmosphere. When the injection rate is increased, it results in the fast migration of carbon dioxide plume within geological formations by invading new and large areas of an aquifer, which causes capillary forces to trap more carbon dioxide gas and brine to dissolve more carbon dioxide. In this study, different injection rates were tested and their results were examined. As shown in Figs. 14, carbon dioxide stored in all forms of storage mechanisms, increased with increasing injection rate and decreased with decreasing injection rate, as shown in Figs. 14. It is recommended to inject carbon dioxide gas at an optimal injection rate to avoid caprock breakdown, which can result in carbon dioxide gas leakage to the surface.

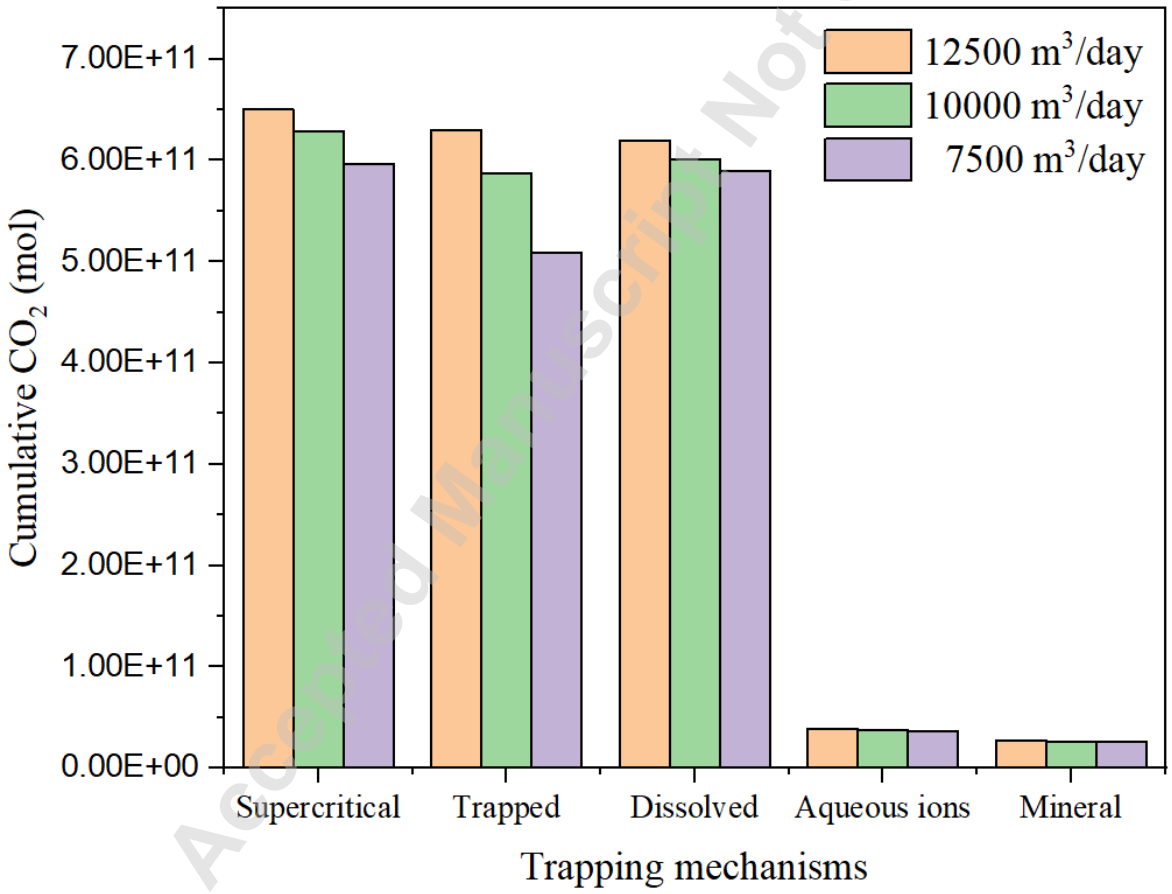


**Fig. 14** Cumulative carbon dioxide stored at different injection rate.

### *3.3 Effects of bottomhole pressure in $CO_2$ sequestration*

In this study, the base bottomhole pressure was 44500 kPa. Different bottomhole pressures were tested to observe their effects on $CO_2$ storage in aquifers by either increasing or decreasing by 25% from the base case. From Fig. 15, it was revealed that as the bottomhole pressure increased, the amount of carbon dioxide stored also increased for all forms of carbon dioxide storage trapping mechanisms. As the bottomhole pressure decreased, the amount of carbon dioxide stored decreased. Specifically, the increase in bottom hole pressure increases the interaction between brine and carbon dioxide gas molecules as well as the lateral movement of carbon dioxide stored in the aquifer. Even if the bottomhole pressure increase showed a positive relationship in all types of storage mechanisms, monitoring and controlling bottomhole pressure remains a very important task in $CO_2$ storage projects because excess bottomhole pressure can result in reservoir pressure buildup that can lead to cap rock leakage, which may result in the escape of $CO_2$ to the surface, especially for gas stored as free gas.

Journal of Energy Resources Technology. Received September 16, 2022;
Accepted manuscript posted December 31, 2022. doi:10.1115/1.4056612


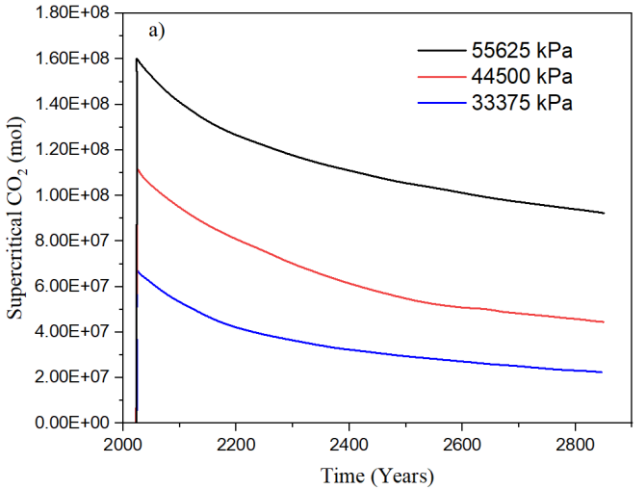


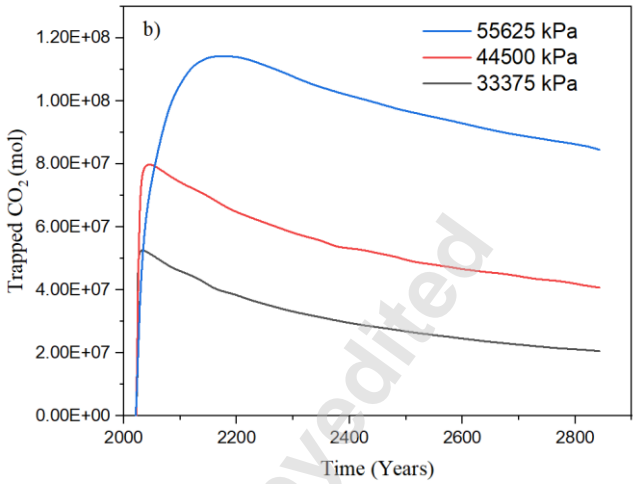


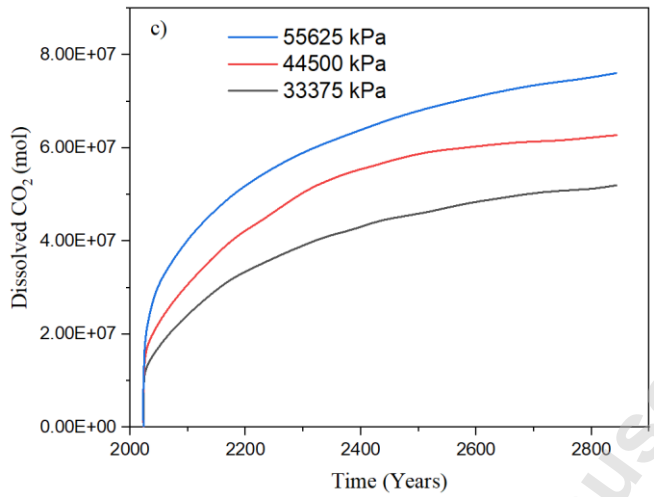


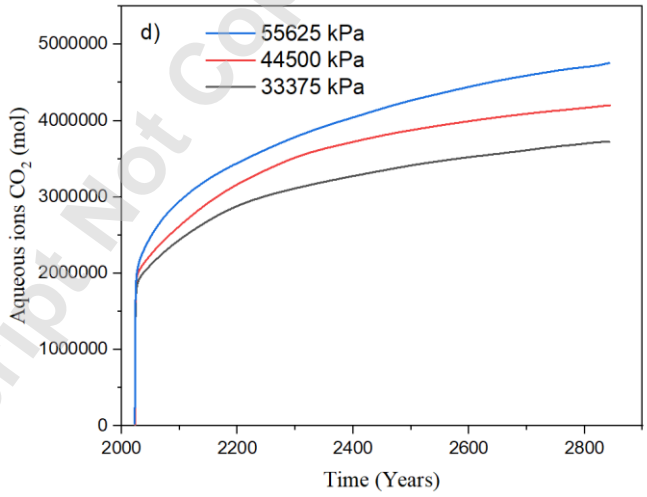


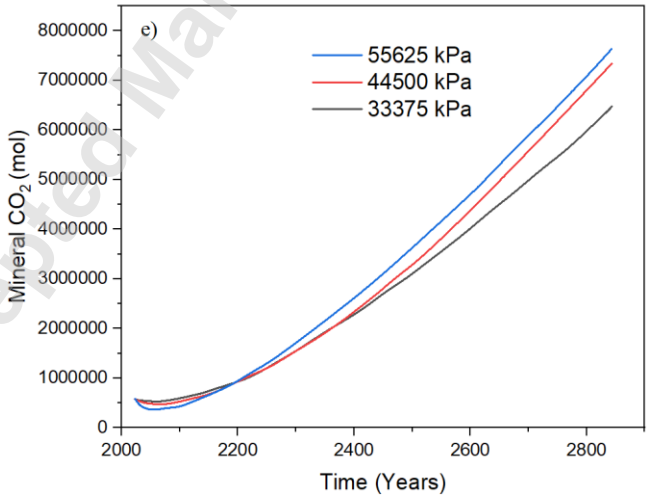

Fig. 15 Effects of bottomhole pressure in different carbon dioxide storage mechanisms

### *3.4 Effects of aquifer temperature in $CO_2$ sequestration*

Aquifer temperatures vary from one aquifer to another depending on different factors such as depositional history, geothermal gradient, geographical location, etc. Aquifer temperature is a very important factor to be taken into account before starting a carbon dioxide storage project. Different aquifers store different amounts of carbon dioxide. High temperatures increase salt precipitation and the rate of reaction. However, high temperatures result in an increase in the relative permeability of carbon dioxide, which might compensate for the permeability reduced due to precipitation of salt. On the other hand, high aquifer temperatures reduce carbon dioxide dissolution, thus reducing aquifer capacity storage. The temperature of the aquifer on $CO_2$ sequestration was examined. Different temperatures were tested to determine the amount of $CO_2$ stored in the aquifer in various forms by either increasing or decreasing by 25%. When the aquifer temperature is higher than the injected carbon dioxide, most of the gas is stored as free gas in caprocks. Because at high temperatures the density of free gas decreases and buoyancy effects dominate, most of the carbon dioxide gas plume moves beyond vertically to the upper layers of the formation, increasing the leakage risk as shown in Fig. 16. Similarly, for mineral trapping mechanisms, it stores more carbon dioxide gas at higher temperatures because of increased chemical reactions and precipitation, although it needs hundreds to thousands of years to take place. Aside from that, higher aquifer temperature has a negative impact on residual, solubility, and aqueous ions trapping mechanisms, i.e., higher aquifer temperature implies less carbon dioxide stored in pore spaces, dissolved in brine, and in aqueous ions form, as illustrated in Fig. 16. This is due to the fact that high temperatures accelerate precipitation and reduce solubility rate, both of which reduce porosity and dissolution. This shows that aquifers with high temperatures are not recommended for carbon dioxide storage projects because most of the gas will be stored in caprocks, which can lead to fractures formation due to thermal expansion and contraction of rocks after carbon dioxide injection, hence carbon dioxide leakage risk increases. Furthermore, higher temperatures reduce the efficiency of most stable trapping mechanisms where carbon dioxide is stored in an immobile phase, i.e., residual and solubility. On the other hand, for mineral trapping mechanisms to become active, it will take a short time to take place for higher temperature aquifers when compared to low temperature aquifers.

Journal of Energy Resources Technology. Received September 16, 2022;
Accepted manuscript posted December 31, 2022. doi:10.1115/1.4056612


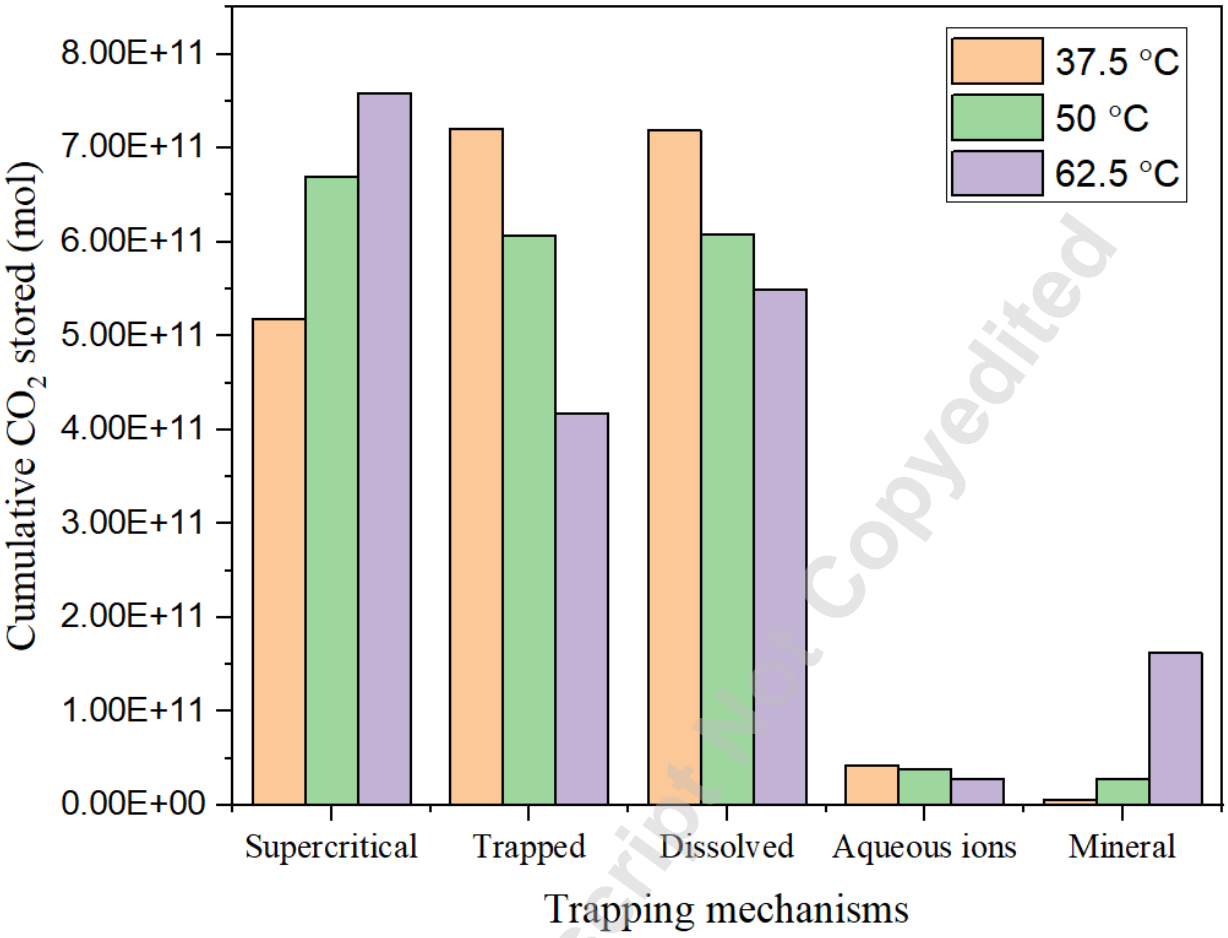


**Fig. 16** Cumulative carbon dioxide stored at different aquifer temperatures.

*3.5 Effects of $k_v/k_h$ ratio in $CO_2$ sequestration*

In this study, variations of vertical to horizontal permeability ($k_v/k_h$ ) ratio were simulated and analyzed in this study in different $CO_2$ trapping mechanisms. The base case $k_v/k_h$ ratio was 1.The minimum $k_v/k_h$ value was set to be 0.1 and the maximum value was 2.Either increasing or decreasing $k_v/k_h$ ratio from base case has shown a directly proportionality to supercritical, and aqueous, mineral carbon dioxide forms of storage trapping mechanisms because there is an increase of vertical $CO_2$ migration in vertical migration and $CO_2$ not get more rooms of contacts with brine. On the other hand, trapped and dissolved mechanisms have shown an inversely proportionality in carbon dioxide storage capacity. i.e, decrease in $k_v/k_h$ ratio led to increase in carbon dioxide dissolved and trapped. This is because less carbon dioxide gas migrates in a vertical direction, thus getting more room to contact the brine and dissolve. Furthermore, lower values of the $k_v/k_h$ ratio cause lateral movements of carbon dioxide, which cause more carbon dioxide to be trapped in more pore spaces . At minimum and maximum $k_v/k_h$ ratios, the amount of carbon

Journal of Energy Resources Technology. Received September 16, 2022;
Accepted manuscript posted December 31, 2022. doi:10.1115/1.4056612


dioxide stored was $5.112 \times 10^{11}$ mol and $8.892 \times 10^{11}$ mol, respectively, compared to the base case of $6.430 \times 10^{11}$ mol at a supercritical state. There was a decrease of 20.5% at the minimum $k_v/k_h$ ratio and an increase of 38.3% at the maximum $k_v/k_h$ ratio of carbon dioxide stored in a supercritical state. Also, the amount of carbon dioxide trapped was $8.402 \times 10^{11}$ mol and $4.878 \times 10^{11}$ mol at minimum and maximum $k_v/k_h$ ratios, respectively. There was an increase of 43.2% and a decrease of 16.84% for minimum and maximum $k_v/k_h$ ratios, respectively, compared to the base case. Further, there was a decrease of carbon dioxide dissolved by 19% $k_v/k_h$ ratios at maximum $k_v/k_h$ ratios and an increase of 58% at minimum $k_v/k_h$ ratios , compared to the base case. Furthermore, there was an increase of carbon dioxide stored in an aqueous state by 5.9% and a decrease of 20.9% at maximum and minimum $k_v/k_h$ ratios, respectively. Apart from that, carbon dioxide stored in mineral forms increased by 3.8% and decreased by 29.7% at maximum and minimum $k_v/k_h$ ratios , respectively, when compared to the base case. Table 8 summarizes the (kv/kh) ratio effects on carbon dioxide stored in various forms of carbon dioxide storage mechanisms.

Table 8. $k_v/k_h$ ratio effects for $CO_2$ storage trapping mechanisms, for 833 years of post-injection

| $k_v/k_h$ ratio | Super-critical $CO_2$ ($\times 10^{11}$) (mol) | Trapped $CO_2$ ($\times 10^{11}$) (mol) | Dissolved $CO_2$ ($\times 10^{11}$) (mol) | Aqueous $CO_2$ ($\times 10^{10}$) (mol) | Mineral $CO_2$ ($\times 10^{10}$) (mol) |
|---|---|---|---|---|---|
| 0.1 | 5.112 | 8.402 | 9.498 | 2.988 | 1.855 |
| 0.2 | 5.298 | 7.886 | 8.501 | 3.209 | 2.121 |
| 0.3 | 5.468 | 7.449 | 8.460 | 3.339 | 2.285 |
| 0.4 | 5.590 | 7.192 | 7.584 | 3.424 | 2.375 |
| 0.5 | 5.876 | 6.935 | 7.102 | 3.509 | 2.464 |
| 0.6 | 5.964 | 6.734 | 6.874 | 3.575 | 2.528 |
| 0.7 | 6.060 | 6.468 | 6.408 | 3.630 | 2.564 |
| 0.8 | 6.123 | 6.368 | 6.279 | 3.670 | 2.600 |
| 0.9 | 6.189 | 6.196 | 6.083 | 3.712 | 2.628 |
| 1 (Base) | 6.430 | 5.866 | 6.010 | 3.778 | 2.639 |
| 1.1 | 6.433 | 5.860 | 5.858 | 3.793 | 2.675 |
| 1.2 | 6.559 | 5.823 | 5.737 | 3.838 | 2.677 |
| 1.3 | 6.690 | 5.684 | 5.618 | 3.850 | 2.696 |
| 1.4 | 7.261 | 5.452 | 5.489 | 3.858 | 2.682 |
| 1.5 | 7.498 | 5.423 | 5.093 | 3.876 | 2.704 |
| 2 | 8.992 | 4.878 | 4.871 | 4.000 | 2.739 |

Journal of Energy Resources Technology. Received September 16, 2022;
Accepted manuscript posted December 31, 2022. doi:10.1115/1.4056612


### *3.6 Effects of salinity in $CO_2$ sequestration*

Salinity was increased and decreased by 50% from the base case. An increase in salinity led to decreased dissolution of gas into brine. As shown in Fig. 17(a), this resulted in an increase in carbon dioxide stored in a supercritical state. Also, because the salinity increase reduces the porosity and permeability of the aquifer, the migration of carbon dioxide is reduced due to clogging of pore throats by salts. This leads to a decrease of carbon dioxide trapped as shown in Fig. 17 (b). On the other hand, because of less dissolution of carbon dioxide into brine, less carbon dioxide is stored in aqueous form when salinity increases, as shown in Fig. 17 (c). Similarly, because more salinity reduces carbon dioxide dissolution in brine, less carbon dioxide is dissolved as shown in Fig. 17 (d). Furthermore, because an increase in salinity reduces the rate of reaction due to less precipitation, the carbon dioxide stored in mineral form is also reduced, as shown in Fig. 17 (e). In general, an increase in salinity decreases the amount of carbon dioxide stored in an aquifer.

Journal of Energy Resources Technology. Received September 16, 2022;
Accepted manuscript posted December 31, 2022. doi:10.1115/1.4056612


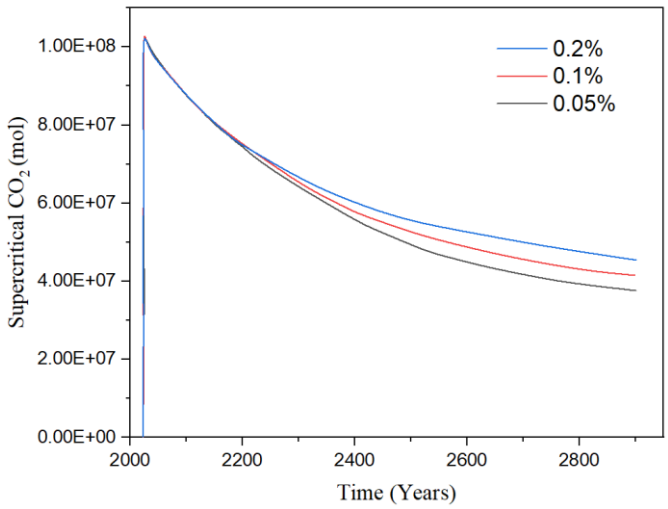


a)

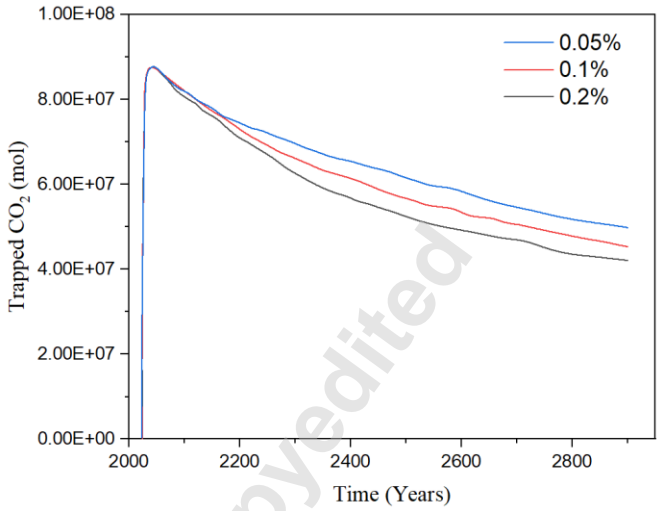


b)

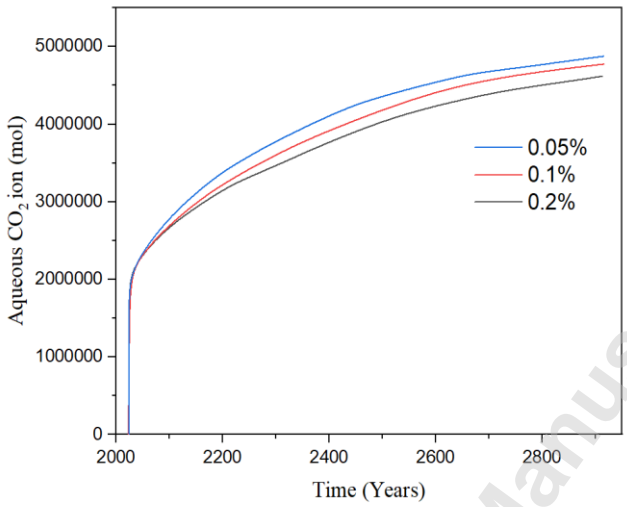


c)

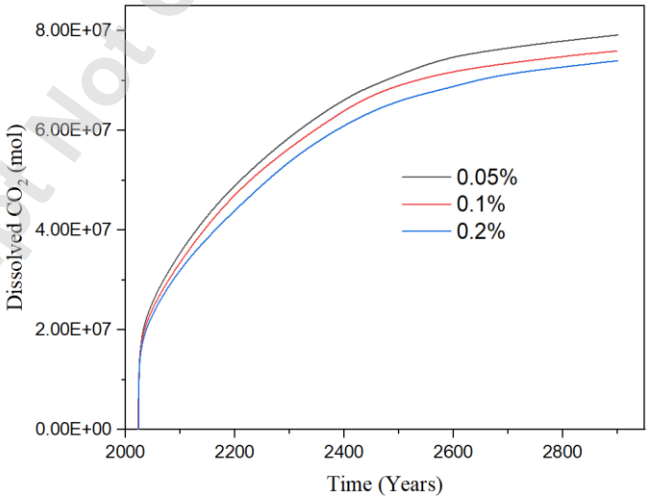


d)

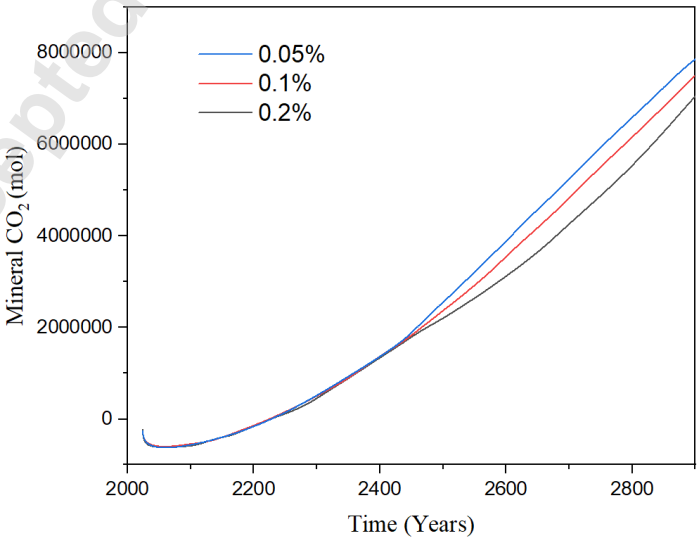


e)

Journal of Energy Resources Technology. Received September 16, 2022;
Accepted manuscript posted December 31, 2022. doi:10.1115/1.4056612


Fig. 17 Effects of salinity in different carbon dioxide storage mechanisms

*3.7 Optimization of residual and solubility trapping mechanisms*

Because residual and solubility are the most important trapping mechanisms in carbon dioxide storage in a deep saline aquifer, and they have been optimized in this study by injecting water above the carbon dioxide injector [43]. The water injection rates tested were 1000 and 2000 $m^3$/day. It was observed that more carbon dioxide was trapped at a higher injection rate (2000 $m^3$/day) than at a lower injection rate (1000 $m^3$/day) as shown in Fig. 18. There was an increase of carbon dioxide trapped by 96.4% when water was injected at a higher rate compared to the base case (no water injection). Similarly, more carbon dioxide was stored in solubility trapping mechanisms when water was injected at a higher injection rate (2000 $m^3$/day) than at a lower injection rate (1000 $m^3$/day) as shown in Fig. 18. There was an increase in carbon dioxide dissolved by 97% when water was injected at a higher rate compared to the base case (no water injection). However, it has been reported that WAG injection with a small WAG ratio is preferred over continuous water injection to enhance residual and solubility trapping mechanisms, as reported by [81] because it reduces leakage risk. But the findings of this study suggest to inject water at a higher rate.

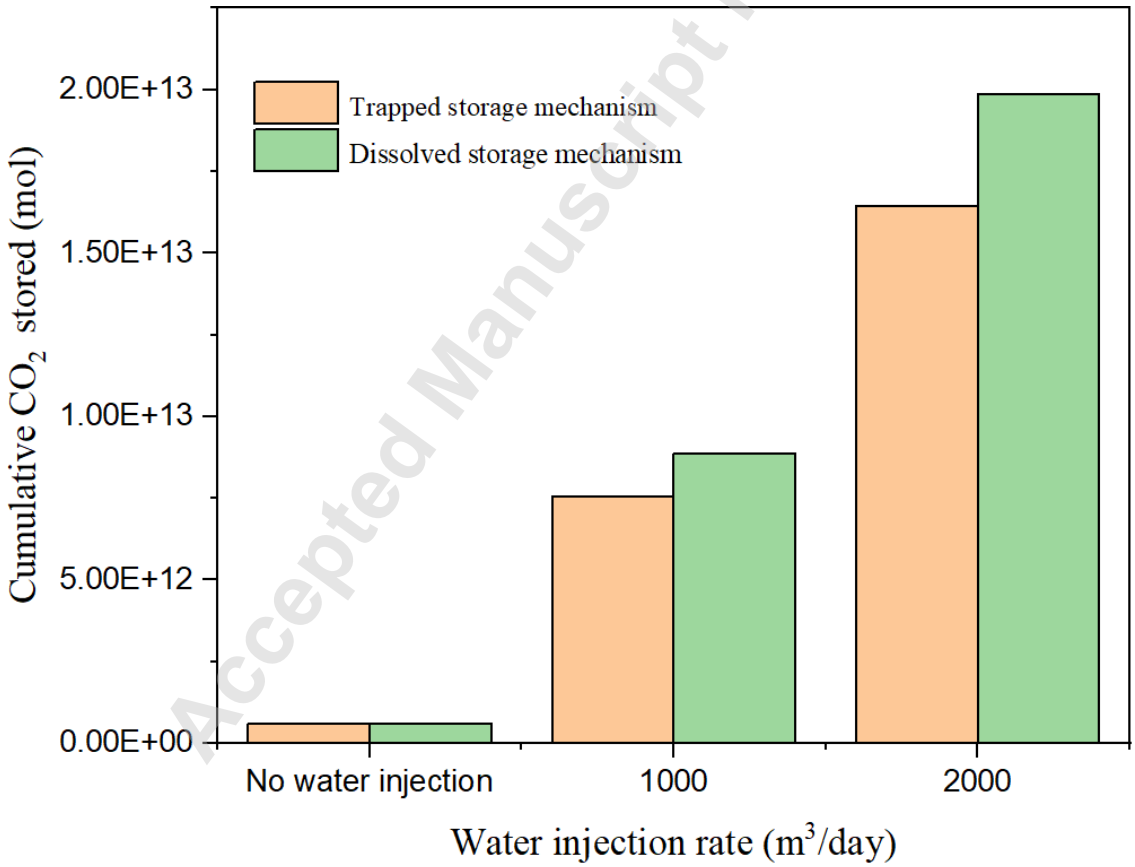

Journal of Energy Resources Technology. Received September 16, 2022;
Accepted manuscript posted December 31, 2022. doi:10.1115/1.4056612


**Fig. 18** Cumulative carbon dioxide stored at different water injection rate.

## 4. Conclusions

Geological carbon dioxide sequestration in aquifers is the main reliable and effective strategy to mitigate global warming effects. However, all the challenges, such as caprock leakage, pressure buildup, earth quake occurrence, crevices during carbon dioxide and post injection, need to be monitored and controlled for a long period of time to avoid carbon dioxide leakage to the surface. In this paper, all the carbon dioxide storage mechanisms, vaporization effects, and residual and solubility trapping optimization were modeled and simulated in a low porosity and permeability deep saline aquifer so as to analyze its capacity for storing carbon dioxide gas. Other findings of this paper are outlined below:

- There was an increase of carbon dioxide trapped by 96.4% and dissolved by 97% when water was injected at a higher rate compared to the base case (no water injection). Thus, a high injection rate is suggested to enhance residual and solubility trapping mechanisms.

- Vertical to horizontal permeability ($k_v/k_h$) ratio has a great influence on carbon dioxide storage in deep saline aquifers and carbon dioxide plume migration. Because residual and solubility trapping mechanisms are the most stable in which carbon dioxide is stored in immobile phase as injection starts, hence deep saline aquifer with low $k_v/k_h$ ratios is recommended and preferred for safe carbon dioxide storage to avoid risk leakages.

- An increase in salinity increases the amount of carbon dioxide stored as free gas because of less dissolution in the brine. However, other forms of carbon dioxide storage, such as residual, dissolved, aqueous, and mineral, are affected inversely by an increase in salinity. Deep saline aquifers with high salinity are not preferred for carbon dioxide storage projects because there is a high risk of carbon dioxide leakage when carbon dioxide is stored in mobile phase (free gas).

- At higher temperatures, less carbon dioxide gas is stored in immobile phase. Hence, higher aquifer temperatures are not recommended for carbon dioxide sequestration. However, the aquifer temperature must be at least as high as the carbon dioxide vaporization temperature (31.05°C).

- An increase in carbon dioxide injection rate increased the amount of carbon dioxide stored in all carbon dioxide storage mechanisms except mineral trapping mechanisms because it takes many years to form minerals after reaction. However, it is recommended that pressure buildup must be controlled and monitored at the well head to avoid caprock breakdown and formation damage.

- Similarly, an increase in bottomhole pressure increased carbon dioxide stored in all forms of carbon dioxide storage trapping mechanisms. However, bottomhole pressure needs to be controlled and monitored to avoid carbon dioxide leakage risks in case there is a mechanical failure in caprocks due to pressure buildup during injection.

This study revealed that low porosity and permeability deep aquifers can store plenty of carbon dioxide gas and should be used as a benchmark for all deep saline aquifers (formations) with low porosity and permeability properties in the Shenhua carbon capture and storage site in the Ordos basin or in another place having similar geological characteristics around the world.

## Data availability statements

Data are available upon reasonable request from corresponding authors

## Acknowledgements

The authors acknowledge supports from Chinese Scholarship Council (2022GXZ005733)

## Conflict of interest

The Authors declare that there is no any conflict of interest

## References

[1] Al Baroudi, H., Awoyomi, A., Patchigolla, K., Jonnalagadda, K., and Anthony, E. J., 2021, "A review of large-scale CO2 shipping and marine emissions management for carbon capture, utilisation and storage," Applied Energy, 287, p. 116510.
[2] Lau, H. C., Zhang, K., Bokka, H. K., and Ramakrishna, S., 2022, "Getting Serious with Net-Zero: Implementing Large-Scale Carbon Capture and Storage Projects in ASEAN," Offshore Technology Conference.
[3] Abdelshafy, A., and Walther, G., 2022, "Coupling carbon capture and utilization with the construction industry: Opportunities in Western Germany," Journal of CO2 Utilization, 57, p. 101866.
[4] Roussanaly, S., Berghout, N., Fout, T., Garcia, M., Gardarsdottir, S., Nazir, S. M., Ramirez, A., and Rubin, E. S., 2021, "Towards improved cost evaluation of Carbon Capture and Storage from industry," International Journal of Greenhouse Gas Control, 106, p. 103263.
[5] Allahyarzadeh-Bidgoli, A., Hamidishad, N., and Yanagihara, J. I., 2021, "Carbon Capture and Storage Energy Consumption and Performance Optimization Using Metamodels and Response Surface Methodology," Journal of Energy Resources Technology, 144(5).
[6] Zhang, Z., Wang, T., Blunt, M. J., Anthony, E. J., Park, A.-H. A., Hughes, R. W., Webley, P. A., and Yan, J., 2020, "Advances in carbon capture, utilization and storage," Applied Energy, 278, p. 115627.
[7] Freire, A. L., José, H. J., and Moreira, R. d. F. P. M., 2022, "Potential applications for geopolymers in carbon capture and storage," International Journal of Greenhouse Gas Control, 118, p. 103687.
[8] Zhang, H., 2021, "Regulations for carbon capture, utilization and storage: Comparative analysis of development in Europe, China and the Middle East," Resources, Conservation and Recycling, 173, p. 105722.
[9] AL-Ameri, W. A., Abdulraheem, A., and Mahmoud, M., 2015, "Long-Term Effects of CO2 Sequestration on Rock Mechanical Properties," Journal of Energy Resources Technology, 138(1).
[10] Rosa, L., and Mazzotti, M., 2022, "Potential for hydrogen production from sustainable biomass with carbon capture and storage," Renewable and Sustainable Energy Reviews, 157, p. 112123.
[11] Ajayi, T., Gomes, J. S., and Bera, A., 2019, "A review of CO2 storage in geological formations emphasizing modeling, monitoring and capacity estimation approaches," Petroleum Science, 16(5), pp. 1028-1063.
[12] Hong, W. Y., 2022, "A techno-economic review on carbon capture, utilisation and storage systems for achieving a net-zero CO2 emissions future," Carbon Capture Science & Technology, 3, p. 100044.
[13] Lau, H. C., Ramakrishna, S., Zhang, K., and Radhamani, A. V., 2021, "The Role of Carbon Capture and Storage in the Energy Transition," Energy & Fuels, 35(9), pp. 7364-7386.
[14] Breault, R. W., and Shadle, L. J., 2018, "Design, Development, and Operation of an Integrated Fluidized Carbon Capture Unit Using Polyethylenimine Sorbents," Journal of Energy Resources Technology, 140(6).

[15] El Fil, B., Hoysall, D. C., and Garimella, S., 2021, "Carbon Dioxide Capture Using Sorbent-Loaded Hollow-Fiber Modules for Coal-Fired Power Plants," Journal of Energy Resources Technology, 144(6).
[16] Mkemai, R. M., and Gong, B., 2020, "Geological performance evaluation of CO2 sequestration in depleted oil reservoirs: A simulation study on the effect of water saturation and vertical to horizontal permeability ratio," Journal of Natural Gas Science and Engineering, 76, p. 103196.
[17] Shukla, R., Ranjith, P., Haque, A., and Choi, X., 2010, "A review of studies on CO2 sequestration and caprock integrity," Fuel, 89(10), pp. 2651-2664.
[18] Kumar, R., Campbell, S. W., and Cunningham, J. A., 2020, "Effect of Temperature on the Geological Sequestration of CO2 in a Layered Carbonate Formation," Journal of Energy Resources Technology, 142(7).
[19] Aminu, M. D., Nabavi, S. A., Rochelle, C. A., and Manovic, V., 2017, "A review of developments in carbon dioxide storage," Applied Energy, 208, pp. 1389-1419.
[20] Chadwick, A., Arts, R., Bernstone, C., May, F., Thibeau, S., and Zweigel, P., 2008, Best practice for the storage of CO2 in saline aquifers-observations and guidelines from the SACS and CO2STORE projects, British Geological Survey.
[21] Li, C., Zhang, K., Guo, C., Xie, J., Zhao, J., Li, X., and Maggi, F., 2017, "Impacts of relative permeability hysteresis on the reservoir performance in CO2 storage in the Ordos Basin," Greenhouse Gases: Science and Technology, 7(2), pp. 259-272.
[22] Okamoto, I., Mito, S., and Ohsumi, T., 2009, "A sensitivity study of CO2 mineralization using GEM–GHG simulator," Energy Procedia, 1(1), pp. 3323-3329.
[23] Zhao, H., Liao, X., Chen, Y., and Zhao, X., 2010, "Sensitivity analysis of CO2 sequestration in saline aquifers," Petroleum Science, 7(3), pp. 372-378.
[24] Kumar, A., Ozah, R., Noh, M., Pope, G. A., Bryant, S., Sepehrnoori, K., and Lake, L. W., 2005, "Reservoir simulation of CO2 storage in deep saline aquifers," Spe Journal, 10(03), pp. 336-348.
[25] Orsini, P., Cantucci, B., and Quattrocchi, F., 2014, "Large-scale numerical modelling of CO2 injection and containment phases for an Italian near-coast reservoir using PFLOTRAN," Energy Procedia, 51, pp. 334-343.
[26] Khan, C., Ge, L., and Rudolph, V., 2015, "Reservoir simulation study for CO2 sequestration in saline aquifers," International Journal of Applied Science and Technology, 5(4), pp. 30-45.
[27] Mo, S., and Akervoll, I., 2005, "Modeling long-term CO2 storage in aquifer with a black-oil reservoir simulator," Spe/epa/doe exploration and production environmental conference, OnePetro.
[28] Ozah, R. C., Lakshminarasimhan, S., Pope, G. A., Sepehrnoori, K., and Bryant, S. L., 2005, "Numerical simulation of the storage of pure CO2 and CO2-H2S gas mixtures in deep saline aquifers," SPE Annual Technical Conference and Exhibition, OnePetro.
[29] Raza, A., Rezaee, R., Bing, C., Gholami, R., Nagarajan, R., and Hamid, M., 2016, "CO2 storage in heterogeneous aquifer: A study on the effect of injection rate and CaCO3 concentration," IOP Conference Series: Materials Science and Engineering, IOP Publishing, p. 012023.
[30] Akai, T., Kuriyama, T., Kato, S., and Okabe, H., 2021, "Numerical modelling of long-term CO2 storage mechanisms in saline aquifers using the Sleipner benchmark dataset," International Journal of Greenhouse Gas Control, 110, p. 103405.
[31] Al-Khdheeawi, E. A., Vialle, S., Barifcani, A., Sarmadivaleh, M., and Iglauer, S., 2017, "Effect of brine salinity on CO2 plume migration and trapping capacity in deep saline aquifers," The APPEA Journal, 57(1), pp. 100-109.
[32] Al-Khdheeawi, E. A., Vialle, S., Barifcani, A., Sarmadivaleh, M., and Iglauer, S., 2018, "The effect of WACO2 ratio on CO2 geo-sequestration efficiency in homogeneous reservoirs," Energy Procedia, 154, pp. 100-105.
[33] Raza, A., Gholami, R., Rezaee, R., Bing, C., Nagarajan, R., and Hamid, M. A., 2017, "CO2 storage in heterogeneous aquifer: A study on the effect of temperature and mineral precipitation," IOP Conference Series: Materials Science and Engineering, IOP Publishing, p. 012002.

[34] Nghiem, L., Shrivastava, V., Kohse, B., Hassam, M., and Yang, C., 2009, "Simulation of trapping processes for CO2 storage in saline aquifers," Canadian International Petroleum Conference, OnePetro.
[35] Nghiem, L., Shrivastava, V., Tran, D., Kohse, B., Hassam, M., and Yang, C., 2009, "Simulation of CO2 storage in saline aquifers," SPE/EAGE reservoir characterization & simulation conference, European Association of Geoscientists & Engineers, pp. cp-170-00063.
[36] Thanh, H. V., Sugai, Y., Nguele, R., and Sasaki, K., 2020, "Robust optimization of CO2 sequestration through a water alternating gas process under geological uncertainties in Cuu Long Basin, Vietnam," Journal of Natural Gas Science and Engineering, 76, p. 103208.
[37] Raza, A., Rezaee, R., Bing, C. H., Gholami, R., Hamid, M. A., and Nagarajan, R., 2016, "Carbon dioxide storage in subsurface geologic medium: A review on capillary trapping mechanism," Egyptian Journal of Petroleum, 25(3), pp. 367-373.
[38] Amin, S. M., Tiwari, R. D., Widyanita, A., Chidambaram, P., Ali, S. S. M., Mazeli, A. H., Tan, C. P., and Hamid, M., 2022, "Impact of karstification in trapping mechanisms of CO2 storage," Journal of Petroleum Exploration and Production Technology, pp. 1-15.
[39] Saraf, S., and Bera, A., 2021, "A review on pore-scale modeling and CT scan technique to characterize the trapped carbon dioxide in impermeable reservoir rocks during sequestration," Renewable and Sustainable Energy Reviews, 144, p. 110986.
[40] Li, X., Akbarabadi, M., Karpyn, Z., Piri, M., and Bazilevskaya, E., 2015, "Experimental investigation of carbon dioxide trapping due to capillary retention in saline aquifers," Geofluids, 15(4), pp. 563-576.
[41] Punnam, P. R., Krishnamurthy, B., and Surasani, V. K., 2022, "Influence of Caprock Morphology on Solubility Trapping during CO2 Geological Sequestration," Geofluids, 2022.
[42] Zhao, X., Liao, X., Wang, W., Chen, C., Rui, Z., and Wang, H., 2014, "The CO2 storage capacity evaluation: Methodology and determination of key factors," Journal of the Energy Institute, 87(4), pp. 297-305.
[43] Nghiem, L., Yang, C., Shrivastava, V., Kohse, B., Hassam, M., Chen, D., and Card, C., 2009, "Optimization of Residual Gas and Solubility Trapping for CO2 Storage in Saline Aquifers," SPE Reservoir Simulation Symposium.
[44] Zhang, Q., and Tutolo, B. M., 2022, "Evaluation of the potential of glauconite in the Western Canadian Sedimentary Basin for large-scale carbon dioxide mineralization," International Journal of Greenhouse Gas Control, 117, p. 103663.
[45] Omari, A., Wang, C., Li, Y., and Xu, X., 2022, "The progress of enhanced gas recovery (EGR) in shale gas reservoirs: A review of theory, experiments, and simulations," Journal of Petroleum Science and Engineering, 213, p. 110461.
[46] Vishal, V., and Singh, T., 2016, "Geologic carbon sequestration," Environ Geosci, 16.
[47] Metz, B., Davidson, O., De Coninck, H., Loos, M., and Meyer, L., 2005, IPCC special report on carbon dioxide capture and storage, Cambridge: Cambridge University Press.
[48] Mkemai, R. M., and Bin, G., 2020, "A modeling and numerical simulation study of enhanced CO2 sequestration into deep saline formation: a strategy towards climate change mitigation," Mitigation and Adaptation Strategies for Global Change, 25(5), pp. 901-927.
[49] Yang, G., Li, Y., Atrens, A., Yu, Y., and Wang, Y., 2017, "Numerical investigation into the impact of CO2-water-rock interactions on CO2 injectivity at the Shenhua CCS demonstration project, China," Geofluids, 2017.
[50] Yu, Y., Li, Y., Yang, G., Jiang, F., Yang, S., and Wang, Y., 2017, "Simulation and analysis of long-term CO2 trapping for the Shenhua CCS Demonstration Project in the Ordos Basin," Geofluids, 2017.
[51] Jing, J., Yang, Y., and Tang, Z., 2021, "Assessing the influence of injection temperature on CO2 storage efficiency and capacity in the sloping formation with fault," Energy, 215, p. 119097.

[52] Yan, W., Ning, W., Yongsheng, W., Maoshan, C., and Xiaochun, L., 2014, "Preliminary cap rock integrity analysis for CO2 geological storage in saline aquifers based on geochemical tests in Shenhua CCS demonstration project, China," Energy Procedia, 63, pp. 2994-2999.
[53] Li, Q., Liu, G., Liu, X., and Li, X., 2013, "Application of a health, safety, and environmental screening and ranking framework to the Shenhua CCS project," International Journal of Greenhouse Gas Control, 17, pp. 504-514.
[54] Nghiem, L., Sammon, P., Grabenstetter, J., and Ohkuma, H., 2004, "Modeling CO2 storage in aquifers with a fully-coupled geochemical EOS compositional simulator," SPE/DOE symposium on improved oil recovery, OnePetro.
[55] Mwakipunda, G. C., Yang, Z., and Guo, C., 2023, "Infill Drilling Optimization for Enhanced Oil Recovery by Waterflooding: A Simulation Study," Journal of Energy Engineering, 149(1), p. 04022053.
[56] Daneshfar, J., Hughes, R. G., and Civan, F., 2009, "Feasibility Investigation and Modeling Analysis of CO2 Sequestration in Arbuckle Formation Utilizing Salt Water Disposal Wells," Journal of Energy Resources Technology, 131(2).
[57] Corey, A. T., 1954, "The interrelation between gas and oil relative permeabilities," Producers monthly, pp. 38-41.
[58] Liu, H., Hou, Z., Were, P., Gou, Y., and Sun, X., 2014, "Simulation of CO2 plume movement in multilayered saline formations through multilayer injection technology in the Ordos Basin, China," Environmental Earth Sciences, 71(10), pp. 4447-4462.
[59] Olabode, A., and Radonjic, M., 2014, "Shale Caprock/Acidic Brine Interaction in Underground CO2 Storage," Journal of Energy Resources Technology, 136(4).
[60] Spiteri, E., Juanes, R., Blunt, M. J., and Orr, F. M., 2005, "Relative-permeability hysteresis: trapping models and application to geological CO2 sequestration," SPE Annual Technical Conference and Exhibition, OnePetro.
[61] Land, C. S., 1968, "Calculation of imbibition relative permeability for two-and three-phase flow from rock properties," Society of Petroleum Engineers Journal, 8(02), pp. 149-156.
[62] Yan, W., Huang, S., and Stenby, E. H., 2011, "Measurement and modeling of CO2 solubility in NaCl brine and CO2–saturated NaCl brine density," International Journal of Greenhouse Gas Control, 5(6), pp. 1460-1477.
[63] Peng, D.-Y., and Robinson, D. B., 1976, "A new two-constant equation of state," Industrial & Engineering Chemistry Fundamentals, 15(1), pp. 59-64.
[64] Nghiem, L., Sammon, P., Grabenstetter, J., and Ohkuma, H., 2004, "Modeling CO2 Storage in Aquifers with a Fully-Coupled Geochemical EOS Compositional Simulator," SPE/DOE Symposium on Improved Oil Recovery.
[65] Azuddin, F. J., Davis, I., Singleton, M., Geiger, S., and Mackay, E., 2020, "Modeling Mineral Reaction at Close to Equilibrium Condition During CO2 Injection for Storage in Carbonate Reservoir," 2020(1), pp. 1-5.
[66] Xu, T., Apps, J. A., and Pruess, K., 2004, "Numerical simulation of CO2 disposal by mineral trapping in deep aquifers," Applied Geochemistry, 19(6), pp. 917-936.
[67] Bachu, S., Gunter, W. D., and Perkins, E. H., 1994, "Aquifer disposal of CO2: Hydrodynamic and mineral trapping," Energy Conversion and Management, 35(4), pp. 269-279.
[68] Gaus, I., Audigane, P., André, L., Lions, J., Jacquemet, N., Durst, P., Czernichowski-Lauriol, I., and Azaroual, M., 2008, "Geochemical and solute transport modelling for CO2 storage, what to expect from it?," International Journal of Greenhouse Gas Control, 2(4), pp. 605-625.
[69] Cantucci, B., Montegrossi, G., Vaselli, O., Tassi, F., Quattrocchi, F., and Perkins, E. H., 2009, "Geochemical modeling of CO2 storage in deep reservoirs: The Weyburn Project (Canada) case study," Chemical Geology, 265(1), pp. 181-197.

[70] Azuddin, F. J., Davis, I., Singleton, M., Geiger, S., Mackay, E., and Silva, D., 2019, "Impact of Temperature on Fluid-Rock Interactions During CO2 Injection in Depleted Limestone Aquifers: Laboratory and Modelling Studies," SPE International Conference on Oilfield Chemistry.
[71] Zuluaga, E., and Lake, L. W., 2004, "Modeling of Experiments on Water Vaporization for Gas Injection," SPE Eastern Regional Meeting.
[72] Dodson, C., and Standing, M., 1944, "Pressure-volume-temperature and solubility relations for natural-gas-water mixtures," Drilling and production practice, OnePetro.
[73] Tang, Y., Yang, R., and Kang, X., 2018, "Modeling the effect of water vaporization and salt precipitation on reservoir properties due to carbon dioxide sequestration in a depleted gas reservoir," Petroleum, 4(4), pp. 385-397.
[74] Vilarrasa, V., and Rutqvist, J., 2017, "Thermal effects on geologic carbon storage," Earth-science reviews, 165, pp. 245-256.
[75] Kaldal, G. S., Jónsson, M. Þ., Pálsson, H., and Karlsdóttir, S. N., 2015, "Structural analysis of casings in high temperature geothermal wells in Iceland," Proceedings of world geothermal congress.
[76] Teodoriu, C., 2013, "Why and when does casing fail in geothermal wells," Oil, Gas, 39.
[77] Zhang, Z., and Agarwal, R., 2013, "Numerical simulation and optimization of CO2 sequestration in saline aquifers," Computers & Fluids, 80, pp. 79-87.
[78] Zhang, Z., and Agarwal, R. K., 2013, "Numerical simulation and optimization of CO2 sequestration in saline aquifers for enhanced storage capacity and secured sequestration," International Journal of Energy and Environment, 4(3), pp. 387-398.
[79] Hassanzadeh, H., Pooladi-Darvish, M., and Keith, D. W., 2009, "Accelerating CO2 dissolution in saline aquifers for geological storage · Mechanistic and sensitivity studies," Energy & Fuels, 23(6), pp. 3328-3336.
[80] Leonenko, Y., and Keith, D. W., 2008, "Reservoir engineering to accelerate the dissolution of CO2 stored in aquifers," Environmental science & technology, 42(8), pp. 2742-2747.
[81] Al-Khdheeawi, E. A., Vialle, S., Barifcani, A., Sarmadivaleh, M., and Iglauer, S., 2018, "Enhancement of CO2 trapping efficiency in heterogeneous reservoirs by water-alternating gas injection," Greenhouse Gases: Science and Technology, 8(5), pp. 920-931.